iScience

CellPress
OPEN ACCESS

Article

Overcoming antibody-resistant SARS-CoV-2 variants with bispecific antibodies constructed using non-neutralizing antibodies

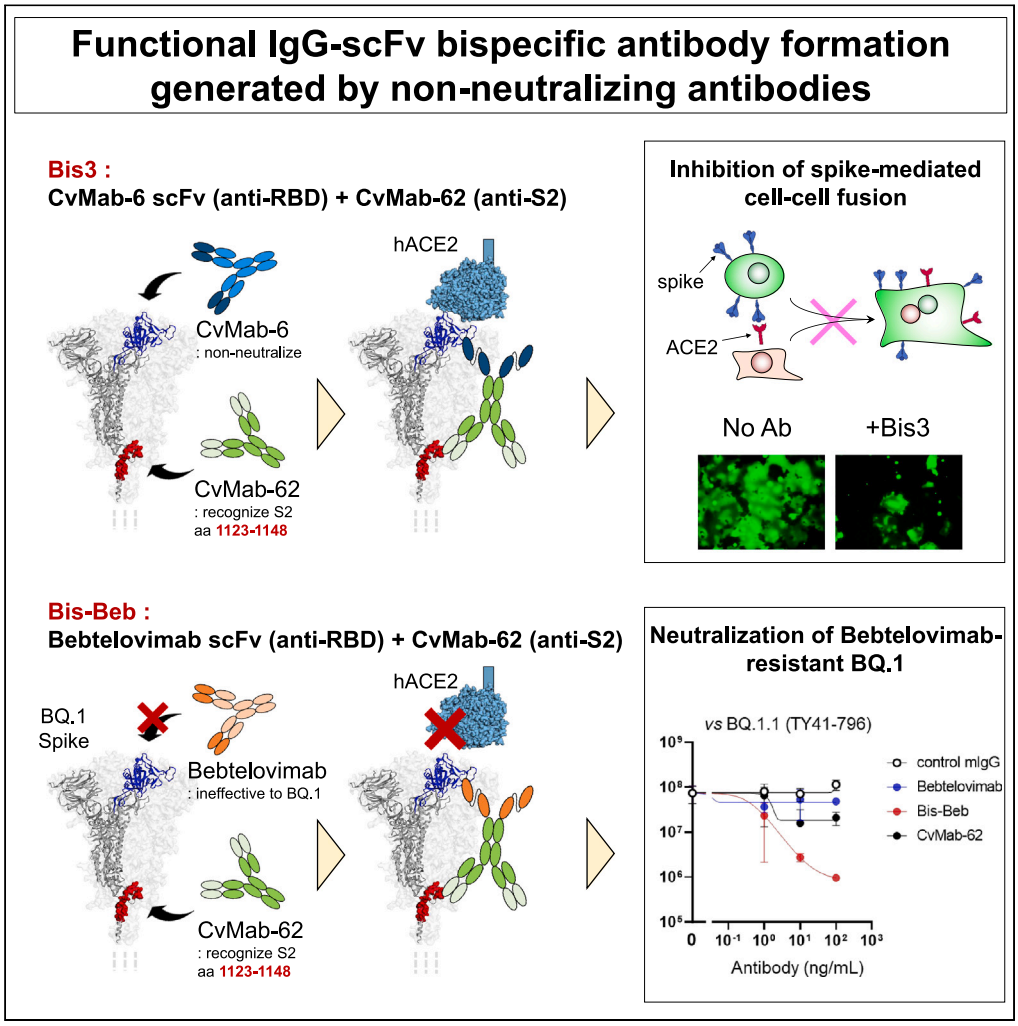

Tetsuya Inoue, Yuichiro Yamamoto, Kaoru Sato, ..., Masayoshi Fukasawa, Yukinari Kato, Kohji Noguchi

fuka@niid.go.jp (M.F.)
yukinari.kato.e6@tohoku.ac.jp (Y.K.)
noguchi-kj@rs.tus.ac.jp (K.N.)

Highlights

Anti-SARS-CoV-2 bispecific Abs can be generated by combining non-neutralizing Abs

Anti-S2 antibody CvMab-62 recognizes a novel epitope upstream of S2 stem helix

Bispecific antibodies can inhibit spike-mediated membrane fusogenic mechanism

Bispecific Abs restore antiviral activity against bebtelovimab-resistant BQ.1.1

Inoue et al., iScience 27, 109363
April 19, 2024
https://doi.org/10.1016/j.isci.2024.109363

iScience

CellPress
OPEN ACCESS

Article

Overcoming antibody-resistant SARS-CoV-2 variants with bispecific antibodies constructed using non-neutralizing antibodies

Tetsuya Inoue,[1] Yuichiro Yamamoto,[1] Kaoru Sato,[1] Yuko Okemoto-Nakamura,[2] Yoshimi Shimizu,[2,3] Motohiko Ogawa,[4] Taishi Onodera,[5] Yoshimasa Takahashi,[5] Takaji Wakita,[6] Mika K. Kaneko,[7,8] Masayoshi Fukasawa,[1,2,*] Yukinari Kato,[7,8,*] and Kohji Noguchi[1,2,9,*]

SUMMARY

A current challenge is the emergence of SARS-CoV-2 variants, such as BQ.1.1 and XBB.1.5, that can evade immune defenses, thereby limiting antibody drug effectiveness. Emergency-use antibody drugs, including the widely effective bebtelovimab, are losing their benefits. One potential approach to address this issue are bispecific antibodies which combine the targeting abilities of two antibodies with distinct epitopes. We engineered neutralizing bispecific antibodies in the IgG-scFv format from two initially non-neutralizing antibodies, CvMab-6 (which binds to the receptor-binding domain [RBD]) and CvMab-62 (targeting a spike protein S2 subunit epitope adjacent to the known anti-S2 antibody epitope). Furthermore, we created a bispecific antibody by incorporating the scFv of bebtelovimab with our anti-S2 antibody, demonstrating significant restoration of effectiveness against bebtelovimab-resistant BQ.1.1 variants. This study highlights the potential of neutralizing bispecific antibodies, which combine existing less effective anti-RBD antibodies with anti-S2 antibodies, to revive the effectiveness of antibody therapeutics compromised by immune-evading variants.

INTRODUCTION

SARS-CoV-2 vaccines, including a new type of mRNA vaccine, have been developed and demonstrated to be highly effective in combating the COVID-19 pandemic. In addition, SARS-CoV-2 RNA polymerase and protease inhibitors have been developed as small-molecule compounds.[1] Specific monoclonal antibodies with virus-neutralizing activity are another powerful approach for the treatment or prevention of SARS-CoV-2 infection.[2–6] SARS-CoV-2 antibody therapeutics demonstrating potent virus neutralization activity have been developed using monoclonal antibodies isolated from the B cells of patients with COVID-19.[7–11] Notably, potent inhibitory antibody therapeutics mostly block the binding between the receptor-binding domain (RBD) of the SARS-CoV-2 spike protein and the cellular receptor angiotensin-converting enzyme 2 (ACE2). These results suggest that the binding interface between ACE2 and the RBD is the optimal target site for potent neutralizing antibodies. Furthermore, neutralizing antibodies that bind to the N-terminal domain or the S2 region of the spike protein have also been identified.[12–16]

Unfortunately, various SARS-CoV-2 variants have acquired immune evasion abilities, even in individuals who have received vaccinations.[17–22] Interestingly, these variants contain amino acid mutations in the RBD that allow the viruses to escape capture by monoclonal antibodies, resulting in antibody resistance. For example, recent Omicron variants, such as BA.4/5 and BA.2.75, have shown resistance to many monoclonal neutralizing antibodies.[23–28] Even bebtelovimab,[29] which remains effective against many variant strains, has seen its effectiveness decreased against the recent variants BQ.1 and XBB.[30,31] The direct correlation between mutations in the RBD-binding site and immune evasion suggests that the most efficient mode of action of neutralizing antibodies, which directly target ACE2-RBD binding, may be the most vulnerable to antibody resistance.

Antibody resistance issues undermine the value of the monoclonal antibodies that have been developed to date and pose a significant obstacle to the development of new monoclonal antibody therapeutics; thus, strategies to overcome it are highly desired. Therefore, it is

[1]Laboratory of Molecular Targeted Therapy, Faculty of Pharmaceutical Sciences, Tokyo University of Science, Yamazaki 2641, Noda, Chiba 278-8510, Japan
[2]Department of Biochemistry and Cell Biology, National Institute of Infectious Diseases, 1-23-1, Toyama, Shinjuku-ku, Tokyo 162-8640, Japan
[3]Department of Pharmaceutical Sciences, Teikyo Heisei University, 4-21-2 Nakano, Nakano-ku 164-8530, Japan
[4]Department of Virology I, National Institute of Infectious Diseases, 1-23-1, Toyama, Shinjuku-ku, Tokyo 162-8640, Japan
[5]Research Center for Drug and Vaccine Development, National Institute of Infectious Diseases, 1-23-1, Toyama, Shinjuku-ku, Tokyo 162-8640, Japan
[6]National Institute of Infectious Diseases, 1-23-1, Toyama, Shinjuku-ku, Tokyo 162-8640, Japan
[7]Department of Molecular Pharmacology, Tohoku University Graduate School of Medicine, 2-1 Seiryo-machi, Sendai, Miyagi 980-8575, Japan
[8]Department of Antibody Drug Development, Tohoku University Graduate School of Medicine, 2-1 Seiryo-machi, Sendai, Miyagi 980-8575, Japan
[9]Lead contact
*Correspondence: fuka@niid.go.jp (M.F.), yukinari.kato.e6@tohoku.ac.jp (Y.K.), noguchi-kj@rs.tus.ac.jp (K.N.)
https://doi.org/10.1016/j.isci.2024.109363

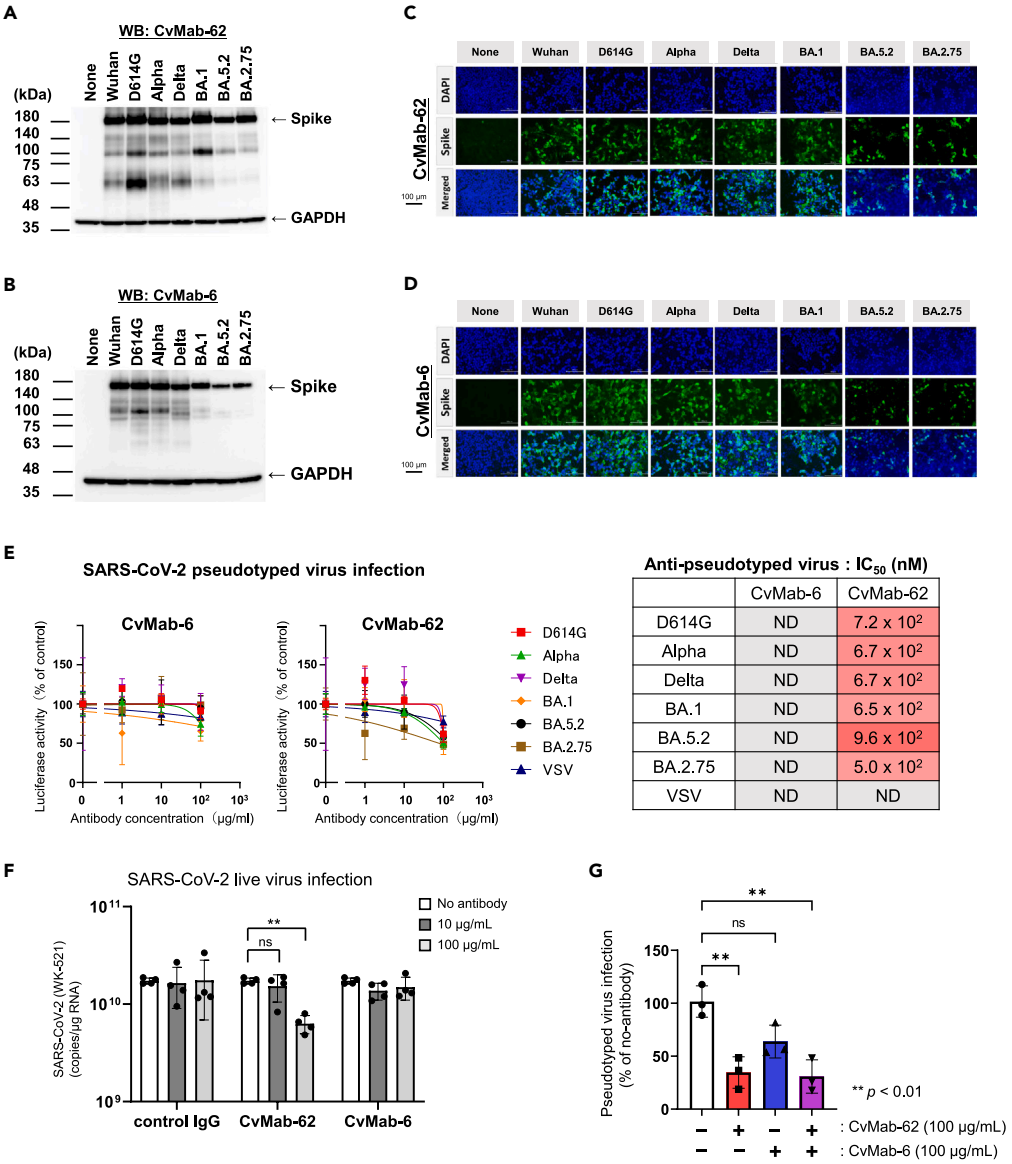

Figure 1. Broad reactivities of anti-S2 CvMab-62 and anti-RBD CvMab-6 antibodies

(A) Western blot analysis using CvMab-62. Spike proteins of Whuan-Hu-1, D614G, Alpha, Delta, Omicron BA.1, BA.5.2 and BA.2.75 expressed in HEK293T cells detected using anti-S2 CvMab-62 antibody.

(B) Western blotting analysis of CvMab-6. Spike proteins of Whuan-Hu-1, D614G, Alpha, Delta, Omicron BA.1, BA.5.2 and BA.2.75 expressed in HEK293T cells detected using anti-RBD CvMab-6 antibody.

(C) Indirect immunofluorescence analysis of CvMab-62. Spike proteins of Whuan-Hu-1, D614G, Alpha, Delta, Omicron BA.1, BA.5.2 and BA.2.75 expressed in HEK293T cells, probed with anti-S2 CvMab-62 antibody, and visualized using secondary anti-mouse IgG-Alexa488 (green signals). Nuclei are counter-stained with DAPI.

(D) Indirect immunofluorescence analysis using CvMab-6. Spike proteins of Whuan-Hu-1, D614G, Alpha, Delta, Omicron BA.1, BA.5.2 and BA.2.75 expressed in HEK293T cells, probed with anti-RBD CvMab-6 antibody, and visualized using secondary anti-mouse IgG-Alexa488 (green signals). Nuclei are counter-stained with DAPI.

(E) Ineffectiveness of CvMab-6 and CvMab-62 against SARS-CoV-2 pseudotyped or control VSV pseudotyped viruses. A pseudotyped virus with a luciferase reporter gene was preincubated with antibodies and used to infect VeorE6/TMPRSS2 cells. The infection ratio was evaluated by measuring cellular luciferase activity 3 days post-infection. Data are presented as the means ± SD (n = 4), and the calculated IC_{50} values are shown in the table on the right.

(F) Non-neutralizing and weak neutralizing activities of CvMab-6 and CvMab-62 against Wuhan-Hu-1 type authentic live SARS-CoV-2 virus. Live SARS-CoV-2 (WK-521) was preincubated with antibodies and used to infect VeroE6/TMPRSS2 cells. The infection ratio was evaluated by measuring cellular viral genomic RNA at one day post-infection using quantitative PCR (n = 4).

Figure 1. *Continued*

(G) No synergy was observed between the CvMab-6 and CvMab-62. Wuhan-type SARS-CoV-2 pseudotyped virus with a luciferase reporter gene was preincubated with either each antibody or a cocktail of antibodies, and VeorE6/TMPRSS2 cells were infected. The infection ratio was evaluated by measuring cellular luciferase activity at 3 days post-infection. Data are presented as the means ± SD (n = 3). Statistical differences were determined using a one-way ANOVA, and a p value <0.05 was considered statistically significant, *p < 0.05, **p < 0.01, ***p < 0.001.

important to explore alternative antibody therapeutics that are based on various mechanisms and innovations. Combining multiple antibodies into a cocktail or creating bispecific or multispecific molecules may enhance the efficacy of antibody therapeutics against viral immune evasion.[32,33] These approaches mitigate the effects of resistance mutations by targeting multiple viral epitopes.

Exploring non-RBD regions or other sites as broad-spectrum neutralizing epitopes is important in research on antibody therapeutics with novel pharmacological actions. With the development of broad-spectrum antibody therapeutics, neutralizing antibodies that target regions with highly conserved cold spots and non-RBD sites in various SARS-CoV-2 strains have been studied. Antibodies targeting the S2 region of the spike protein, specifically the highly conserved stem helix region, show relatively broad neutralizing activity, although their inhibitory activity is weaker than that of many RBD-binding neutralizing antibodies.[34–41] To overcome the weaknesses of non-RBD-targeting antibodies, recombinant antibodies can be created by combining them with other molecules to generate powerful inhibitory activity against viral infection. Furthermore, bispecific antibodies that combine with non-neutralizing epitopes are promising therapeutic antibodies.[42,43] These strategic concepts have the potential to generate a diverse range of SARS-CoV-2–neutralizing antibodies with various pharmacological mechanisms. This approach is expected to be effective in combating the emergence of immune evasion mutations.

In this study, we developed bispecific neutralizing antibodies by combining two types of non-neutralizing antibodies that do not directly inhibit the binding of the spike protein to ACE2: one antibody binds to the RBD but lacks neutralizing activity, and the other targets a highly conserved epitope in the S2 region. This approach led to the discovery of a clone with enhanced inhibitory effects and broad-spectrum infection-blocking activity. Moreover, we combined the single-chain variable fragment (scFv) of bebtelovimab, which is a therapeutic anti-RBD antibody[29] that had become ineffective owing to the emergence of the resistant variants BQ.1 and XBB,[30,31] with our anti-S2 antibody CvMab-62. We found that this bispecific antibody overcame the resistance of BQ.1.1 to bebtelovimab. Thus, bispecific antibodies combining the S2 antibody with other RBD-targeting antibodies may be a promising and optional module to restore efficacy against antibody-resistant SARS-CoV-2 variants.

RESULTS

Bispecific antibodies were generated from the combination of the non-neutralizing anti-RBD antibody CvMab-6 and anti-S2 antibody CvMab-62

It has been reported that bispecific antibodies, combined with non-neutralizing antibodies that recognize highly conserved regions, demonstrate broad neutralizing activity.[42] Furthermore, bispecific antibodies that recognize both the RBD and S2 regions have been reported to exhibit better neutralizing activity than their parental monoclonal antibodies.[44] Therefore, we generated anti-SARS-CoV-2 bispecific antibodies from non-neutralizing anti-RBD and anti-S2 antibodies.

CvMab-6 targeting RBD and CvMab-62 targeting S2 were broadly reactive antibodies, and their binding to spike proteins of variants including the Wuhan strain, D614G, Alpha, Delta, and Omicron BA.1, BA.5.2, and BA.2.75 were confirmed by western blot and indirect immunofluorescence analyses (Figures 1A–1D, respectively). From the western blot analysis, we observed less fragmentation of the full length omicron spike proteins, which aligns with the results of previous reports.[45,46] The anti-S2 antibody, CvMab-62, but not the anti-RBD antibody, CvMab-6, showed weak but selective inhibition against pseudotyped and authentic SARS-CoV-2 infections only at high concentrations (Figures 1E and 1F). The combination of CvMab-6 and CvMab-62 showed no synergistic effects (Figure 1G). These results indicated that the anti-S2 antibodies CvMab-62 and anti-RBD CvMab-6 are non-neutralizing antibodies compared to the previously reported neutralizing antibodies.

The CvMab-6 epitope corresponds to amino acids 459–478 of the spike protein, determined by an enzyme-linked immunosorbent assay (ELISA) using a synthetic series of SARS-CoV-2-S1-RBD peptides, as shown in Table S1. The amino acid sequence at 459–478 is highly conserved in SARS-CoV-2 and bat RaTG13 spike proteins but not in the spike protein of another bat species, Khosta-2 (Figure 2A). Consistently, CvMab-6 recognized the bat coronavirus RaTG13 spike protein but did not react with the bat coronavirus Khosta2 spike protein (Figures 2B and 2C, respectively). This region was not the binding interface between ACE2 and RBD (Figure 2D), and consistently CvMab-6 did not inhibit ACE2-RBD binding in ELISAs (Figure 2E), confirming that CvMab-6 is a non-neutralizing antibody. Consistent with the results shown in Figures 1B and 1D, the amino acid sequence corresponding to the CvMab-6 epitope was highly conserved among SARS-CoV-2 variants (Figure 2F).

The CvMab-62, an anti-S2 antibody, also showed weak reactivity toward Khosta-2, unlike the control anti-S2 antibody 1A9 which recognizes the highly conserved region, Wuhan-Hu-1 spike protein at amino acids position 1029–1192 (Figures 2G and 2J). As summarized in Figures 2I and S1, western blot analysis using the deletion mutants of the S2 protein revealed that CvMab-62 did not interact with the mutants lacking residues 1070–1162. The spike protein of bat Khosta2 differs from SARS-CoV-2 in the corresponding 1070–1162 residue region due to amino acid substitutions such as A1070S, E1072D, D1084K, H1088Y, S1097T, E1111Q, Q1113E, I1114V, D1118E, V1122E, and D1146E (Figure 2J), and additional western blot analyses revealed that mutations A1070S, E1072D, D1084K/H1088Y, QPEV (E1111Q/Q1113E/I1114V), the deletion from 1085 to 1122 and the deletion from 1149 to 1162 do not impact CvMab-62 binding, but D1146E mutation disrupts CvMab-62 binding (Figure S1). In addition, the binding of CvMab-62 to the S2 region does not require the presence of residues

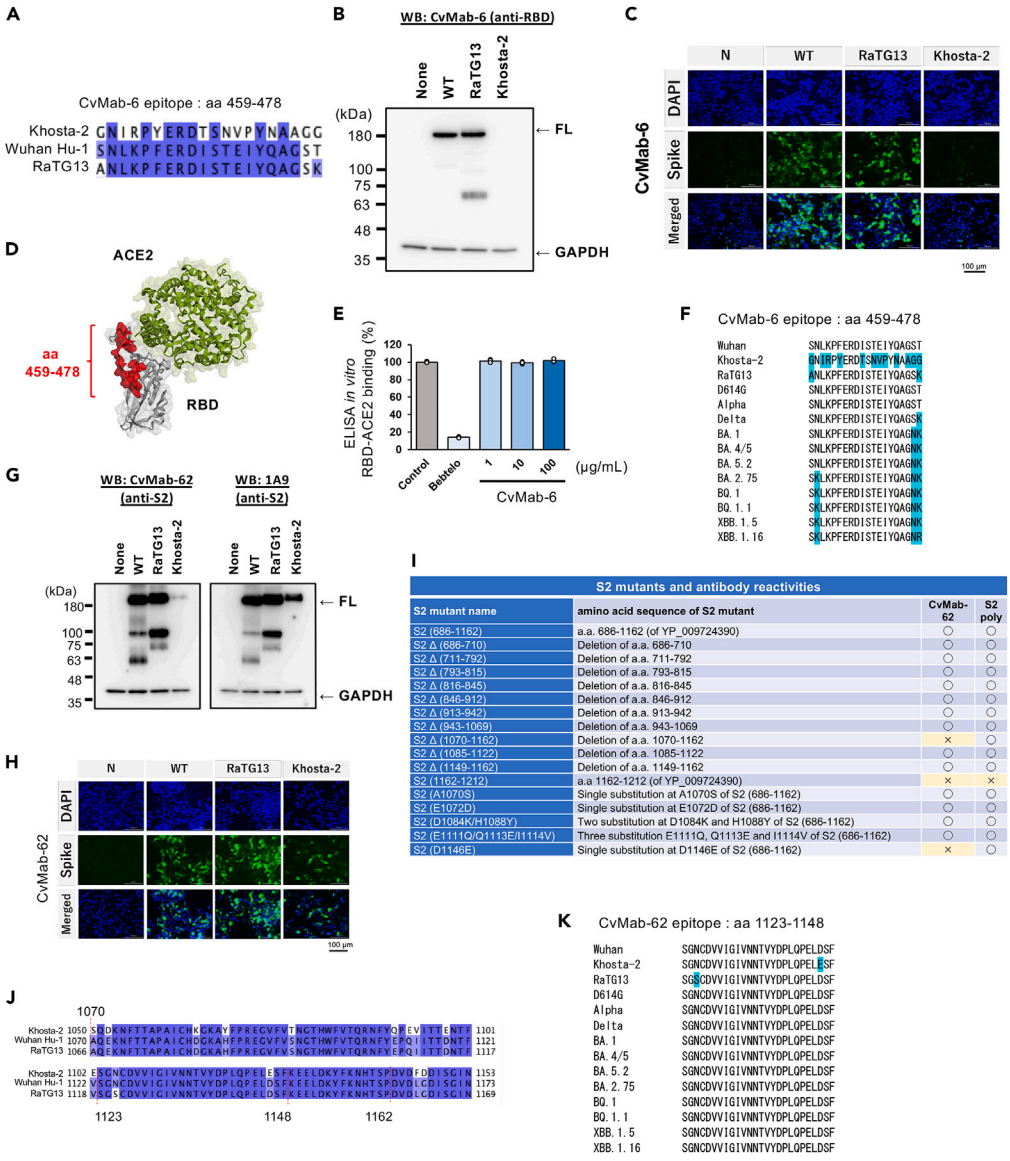

Figure 2. Anti-RBD CvMab-6 and anti-S2 CvMab-62 epitopes

(A) Amino acid alignment of CvMab-6 target element. Amino acid residues corresponding to position 459–478 of the Wuhan-Hu-1 spike protein are aligned with those of bat coronaviruses RaTG13 and Khosta2.

(B) Western blot analysis of CvMab-6 on bat coronavirus spike proteins. CvMab-6 did not react with the Khosta2 spike protein.

(C) Indirect immunofluorescence analysis of CvMab-6 on bat coronavirus spike proteins. CvMab-6 did not react with the Khosta2 spike protein expressed in HEK293 cells.

(D) Structural model of the CvMab-6 target element. The red region represents the CvMab-6 binding site.

(E) CvMab-6 did not inhibit RBD-ACE2 binding. Preincubation of RBD with bebtelovimab, but not with CvMab-6, inhibited *in vitro* binding between RBD and ACE2 using ELISA. Data are presented as the means ± SD (n = 3).

(F) Amino acid alignment of the CvMab-6 target element corresponding to positions 459–478 of the several variant spike proteins. Light blue indicates mutated amino acids.

(G) Western blot analysis of CvMab-62 on bat coronavirus spike proteins. The reactivity of CvMab-62 with the Khosta2 spike protein was strongly reduced compared to the anti-S2 1A9 antibody.

(H) Indirect immunofluorescence analysis showed reduced reactivity of CvMab-62 on bat coronavirus Kohosta2 spike proteins expressed in HEK293T cells.

(I) Summary of western blot analysis of the deletion mutant S2 proteins using CvMab-62. CvMab-62 detected a deletion mutant S2 protein lacking amino acid residues 1149–1162, but did not react with the D1146E mutant S2 protein.

(J) Amino acid alignments of corresponding to positions 1070–1173 of the Wuhan-Hu-1 spike protein were aligned with those of bat coronaviruses RaTG13 and Khosta2.

(K) Amino acid alignments of the CvMab-62 target element corresponding to positions 459–478 of the several variant spike proteins. Light blue indicates mutated amino acids.

1149–1162 (KEELDKYFKNHTSP), a common epitope for most anti-S2 neutralizing antibodies,[34,47] indicating that the CvMab-62 epitope is novel within the region of residues 1123–1148, with a particular focus on D1146.

Four IgG-type bispecific antibodies were tested using the original CvMab-6 and CvMab-62 antibodies. Bis1 was generated by fusing the scFv of CvMab-62, which recognizes S2, to the C-terminus of the heavy chain of cCvMab-6, whereas Bis2 was generated by fusing it to the C-terminus of the light chain of cCvMab-6. Bis3 was generated by fusing the scFv of cCvMab-6, which recognizes the RBD, to the C-terminus of the heavy chain of CvMab-62, and Bis4 was generated by fusing it to the C-terminus of the light chain of CvMab-62 (Figure 3A). Purified recombinant antibodies were confirmed using SDS-PAGE and Coomassie brilliant blue staining (Figure 3B). The dual-binding activity of these bispecific antibodies was confirmed by ELISA (Figure S2), and the binding affinities of each recombinant antibody toward the monomeric RBD alone (Figure 3C) and trimeric ectodomain of the spike protein (Figure 3D) were evaluated by ELISA. The binding affinity of Bis1 was lower than that of the parental antibodies CvMab-6 and CvMab-62, whereas the binding affinity of Bis2 was comparable to that of the anti-RBD antibody CvMab-6 (Figure 3D). In contrast, Bis3 and Bis4 exhibited binding affinities to the trimeric ectodomain of the spike protein at a level similar to those of the anti-S2 antibody CvMab-62 (Figure 3D, right table), and their binding affinities to the RBD were comparable to that of CvMab-6 (Figure 3C, bottom table). As expected, these bispecific antibodies did not inhibit *in vitro* binding between the RBD and ACE2 (Figure S3). However, when the antiviral activity of these bispecific antibodies was examined in a pseudotyped virus assay, Bis3 showed the strongest inhibitory activity against the Wuhan, Alpha, Delta, and BA.1 variants (Figure 3E). The IC_{50} value of Bis3 was lower than that of the parental CvMab-62, indicating improved neutralizing activity through bispecific antibody formation. Furthermore, we evaluated the inhibitory activity against SARS-CoV-2 live virus infection, and similarly, Bis3 exhibited the strongest inhibition against the Wuhan, Alpha, Delta, and BA.1 strains among the four types of bispecific antibodies (Figure 3F). These results demonstrate that bispecific antibodies combining non-neutralizing antibodies, particularly those based on S2 antibodies, such as Bis3, can generate antiviral activity.

In order to confirm the role of CvMab-62 binding to its epitope for the neutralizing activity of bispecific antibody, *in vitro* bindings experiment was conducted and result showed that the bindings of CvMab-62 to trimeric BA4/5 and BQ.1 ectodomain were completely canceled by 1 μM peptide (called D1146 peptide, corresponding to the CvMab-62 epitope, a.a 1131–1148, GIVNNTVYDPLQPELDSF), but not by a D1146E mutated peptide (called E1146 peptide) (Figure 4A). The bindings of the anti-RBD antibody bebtelovimab to the spike ectodomains was not affected by these S2 peptides. Western blot analysis confirmed that the D1146E mutation disrupted the recognition of spike protein by CvMab-62 (Figure 4B), and consistently Bis3 was shown not to inhibit D1146E-mutated pseudotyped virus infection (Figure 4C). These results confirmed that CvMab-62-binding to its epitope is actually required for bispecific antibody-mediated neutralizing activity.

The bispecific antibody Bis3 can inhibit endocytosis-associated viral infection and spike-mediated cell-cell fusion

Regarding the viral entry mechanism, SARS-CoV-2 has two cell entry routes[48]: transmembrane serine protease 2 (TMPRSS2)-dependent cell surface-membrane fusion and TMPRSS2-independent endocytosis (Figure S4). SARS-CoV-2 Omicron variants are thought to be endocytosis pathway dominant types.[45,49–51] HEK293/ACE2 cells, expressing little TMPRSS2, possess mainly TMPRSS2-independent endocytic pathways, whereas VeroE6/TMPRSS2 cells[52] appear to possess both pathways. When the effect of bispecific antibodies on the endocytosis-mediated viral entry pathway was examined in HEK293/ACE2 cells, Bis3 showed an antiviral effect against BA.1 and BA.5.2 pseudotyped viruses (Figure 5A, lower graphs). In contrast, BA.2.75 pseudotyped virus infection in either VeroE6/TMPRSS2 or HEK293/ACE2 was not inhibited by Bis3, suggesting that BA.2.75 spike-mediated infection is resistant to Bis3. Overall, our results indicate that Bis3 inhibits the TMPRSS2-independent endocytic pathway.

When two antibodies, an anti-S2 and an anti-RBD antibody, which cannot directly inhibit the binding between the RBD of the spike protein and its receptor ACE2, were combined as Bis3, the inhibitory effect on infection was enhanced. However, the mechanism underlying this enhancement remains unclear. Previous studies have suggested that inhibition of the membrane fusion step mediated by the S2 region of the spike protein is a mechanism for infection inhibition by anti-S2 antibodies.[34] Therefore, a cell-cell fusion assay was conducted using HEK293 cells expressing the Wuhan-type, Omicron BA.1, BA.5.2, or BA. 2.75 strain spike protein, and VeroE6/TMPRSS2 cells, to investigate the effect of bispecific antibodies on cell membrane fusion. The results demonstrated that each of the four bispecific antibodies showed varying degrees of inhibitory effects on cell-cell fusion. In particular, Bis3 exhibited significantly strong inhibitory activity to cell-cell fusion of Wuhan-type, BA.1, and BA.5.2 (Figures 5B and 5C). Cell-cell fusion induced by the BA.1 spike protein was susceptible to all four bispecific antibodies, consistent with the results of infection inhibition experiments using BA.1 pseudotyped virus and live virus (Figures 3E and 3F). The spike proteins of BA.5.2 showed weak but Bis3-sensitive cell-cell fusion activity, whereas BA.2.75 showed little cell-cell fusion activity in this setting (Figure 5C). The low fusogenic activity observed for BA.2.75 spike protein may potentially exhibit a correlation with resistance to Bis3. Taken together, these results indicate that Bis3 targets the fusogenic activity of spike proteins.

Bispecific antibody Bis3 does not inhibit TMPRSS2-mediated spike cleavage

SARS-CoV-2 spike-mediated infection involves TMPRSS2-dependent spike protein cleavage into the S1 and S2 portions. We examined the effect of Bis3 treatment on TMPRSS2-dependent spike protein cleavage during cell-cell fusion. In this study, the split green fluorescent protein (GFP) technique was introduced into the cell-cell fusion assay.[53,54] When GFP 1-10- and spike-expressing HEK293 cells were fused with GFP11-, ACE2-, and TMPRSS2-expressing HEK293 cells, the GFP signal was restored in the fused giant cells (Figure 6A). The inhibitory effect of Bis3-pretreatment on this GFP-signal ratio was measured, and the results showed that Bis3 significantly inhibited TMPRSS2-dependent and -independent GFP signaling, while CvMab-6 and CvMab-62 showed no effect (Figures 6B and 6C). Spike protein cleavage was then examined by western blot analysis, probing the S2 fragment cleaved at the Ser-686 position, showing that Bis3 treatment did not suppress

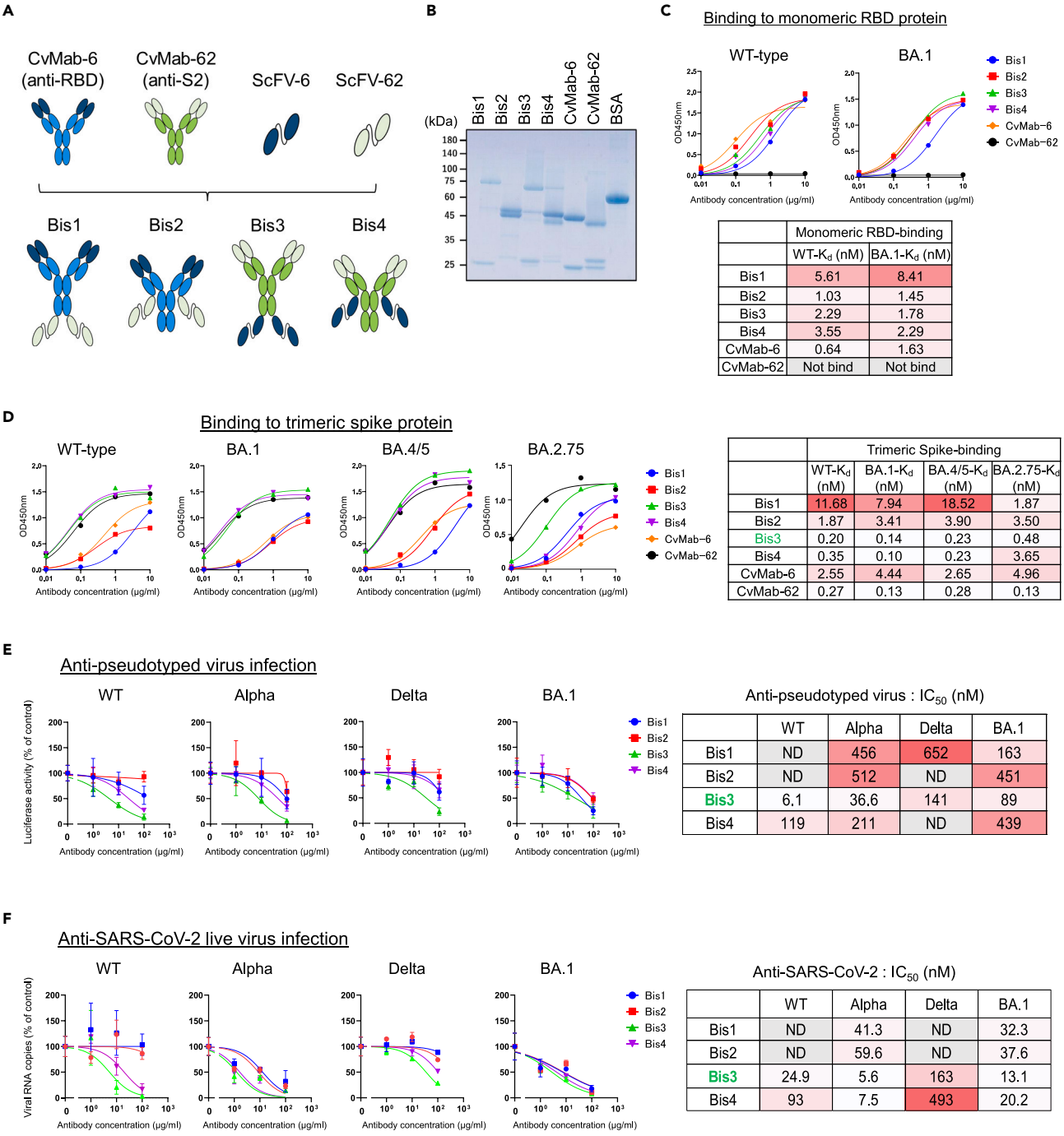

	Monomeric RBD-binding	
	WT-K_d (nM)	BA.1-K_d (nM)
Bis1	5.61	8.41
Bis2	1.03	1.45
Bis3	2.29	1.78
Bis4	3.55	2.29
CvMab-6	0.64	1.63
CvMab-62	Not bind	Not bind

	Trimeric Spike-binding			
	WT-K_d (nM)	BA.1-K_d (nM)	BA.4/5-K_d (nM)	BA.2.75-K_d (nM)
Bis1	11.68	7.94	18.52	1.87
Bis2	1.87	3.41	3.90	3.50
Bis3	0.20	0.14	0.23	0.48
Bis4	0.35	0.10	0.23	3.65
CvMab-6	2.55	4.44	2.65	4.96
CvMab-62	0.27	0.13	0.28	0.13

Anti-pseudotyped virus : IC_{50} (nM)

	WT	Alpha	Delta	BA.1
Bis1	ND	456	652	163
Bis2	ND	512	ND	451
Bis3	6.1	36.6	141	89
Bis4	119	211	ND	439

Anti-SARS-CoV-2 : IC_{50} (nM)

	WT	Alpha	Delta	BA.1
Bis1	ND	41.3	ND	32.3
Bis2	ND	59.6	ND	37.6
Bis3	24.9	5.6	163	13.1
Bis4	93	7.5	493	20.2

Figure 3. Anti-SARS-CoV-2 effects of bispecific antibodies

(A) Schematic of bispecific antibodies. The scFv of anti-S2 CvMab-62 was fused to the C-terminus of anti-RBD CvMab-6 heavy (Bis1) or light (Bis2) chains. Conversely, the scFv of anti-RBD CvMab-6 was fused to the C-terminus of the anti-S2 CvMab-62 heavy (Bis3) or light (Bis4) chains.

(B) The presence of recombinant bispecific antibodies was confirmed by SDS-PAGE, followed by Coomassie blue staining.

(C) In vitro binding of bispecific antibodies to monomeric RBD consists of amino acids 319–541, measured by ELISA. The RBD protein (WT: Wuhan type, or BA.1) was coated in the wells, and bispecific antibodies at the indicated concentrations were added. The calculated KD values using GraphPad Prism9 are presented in the table below.

(D) *In vitro* binding of bispecific antibodies to the trimeric spike ectodomain, was measured using ELISA. The trimeric spike ectodomain proteins (WT: Wuhan type, BA.1, BA.5.2, or BA.2.75) were coated onto the wells, and bispecific antibodies at the indicated concentrations were added. The KD values, calculated using GraphPad Prism9 are presented in the table on the right.

Figure 3. *Continued*

(E) Neutralization of bispecific antibodies against SARS-CoV-2 pseudotyped viruses. Pseudotyped viruses were preincubated with antibodies at the indicated concentrations and then used to infect VeroE6/TMPRSS2 cells. Three days post-infection, cellular luciferase activity was measured to estimate the pseudotyped virus infection ratio. Data are presented as the means ± SD (n = 3). The inhibitory effects of the bispecific antibodies are shown as IC_{50} values summarized in the table on the right side. ND: not determined.

(F) Neutralization activity of bispecific antibodies against authentic SARS-CoV-2 viruses. Authentic SARS-CoV-2 variant viruses were preincubated with antibodies at the indicated concentrations and then used to infect VeroE6/TMPRSS2 cells. At 24 h post-infection, viral genomic RNA in cells was measured by quantitative RT-PCR, and viral replication was shown as the ratio of the control. Data are presented as the means ± SD (n = 4). The inhibitory effects of the bispecific antibodies are shown as IC_{50} values summarized in the table on the right side. ND: not determined.

TMPRSS2-dependent S2 fragment production (Figure 6D, upper panels). Collectively, these data indicated that Bis3 did not interfere with TMPRSS2-dependent spike cleavage during cell-cell fusion, suggesting that Bis3 targets the spike S2 fragment-mediated fusion process downstream of TMPRSS2-dependent spike protein cleavage (Figure 6E).

Bispecific antibody Bis-Beb restores binding ability to BQ.1.1

Bebtelovimab is a broadly reactive neutralizing antibody effective against many SARS-CoV-2 variants.[55] However, its efficacy has diminished against recent variants such as BQ.1 and XBB1.5.[26,30,31,56] Specifically, the effectiveness of bebtelovimab depends on the binding of K444 in the RBD recognition mode (Figure 7A), and it becomes ineffective in cases, such as BQ1.1, with the K444T mutation.[30] Bispecific antibodies hold promise for overcoming antibody resistance as they can target multiple epitopes. Therefore, to overcome antibody resistance, we developed a novel bispecific antibody, Bis-Beb (Figure 7B). This was accomplished by integrating the antigen-recognition site of bebtelovimab in the form of an scFv into our anti-S2 antibody, CvMab-62, similar to the approach used for Bis3. To validate the binding of this bispecific antibody to the spike protein of BQ1.1, we conducted an ELISA. The Bis-Beb Kd value for the BQ.1.1 trimeric spike ectodomain was more than ten times lower than that of bebtelovimab, whereas the Kd value for the BA4/5 trimeric spike ectodomain was similar to that of the original antibody, bebtelovimab (Figures 7C–7E). Binding of CvMab-62 to the BA4/5 and BQ.1.1 trimeric spike ectodomains were comparable.

Surface Plasmon Resonance (SPR) experiments were conducted to assess the binding strength between Bis-Beb and the spike ectodomain (Figure 7F). In these SPR experiments, we investigated the binding of antibodies with the BQ.1.1 and BA.4/5 trimeric ectodomains under two different pH conditions: neutral (pH 7.4) and acidic (pH 5.5), which served as a representative model for the acidic milieu typically encountered within endosomes. Bis-Beb exhibited strong and stable binding of BQ.1.1 to the BA.4/5 ectodomain under both pH conditions (red lines). In contrast, the original bebtelovimab showed strong binding to the BA4/5 ectodomain, but it rapidly dissociated from the BQ.1.1 ectodomain at pH 7.4. At pH 5.5, it exhibited a complete lack of binding interaction (blue lines). Similar to Bis-Beb, CvMab-62 exhibited strong and stable binding under both conditions (black lines). These results highlight that bebtelovimab has weak binding to BQ.1.1, particularly under acidic conditions, while the bispecific antibody Bis-Beb exhibits strong and stable binding similar to its parent, CvMab-62, toward both BQ.1.1 and BA.4/5.

Bispecific antibodies overcome bebtelovimab resistance

Figure 7 shows that Bis-Beb exhibited a stronger binding affinity to the trimeric BQ.1.1 spike ectodomain than bebtelovimab. However, the *in vitro* binding of Bis-Beb to monomeric BQ.1 RBD was weaker than that of bebtelovimab (Figure 8A), suggesting that the scFv format of bebtelovimab decreased its binding affinity to the RBD of BQ.1. To investigate whether the combination of CvMab-62's Fab and bebtelovimab's scFv exhibits an enhancing effect on the binding of the bispecific antibody to the spike protein, binding inhibition experiments were conducted using the CvMab-62's epitope peptide via ELISA (Figure 8B). Upon comparing the IC_{50} values for the binding inhibition activity of this peptide, it was demonstrated that the binding of Bis-Beb to the trimeric BQ.1 ectodomain was approximately 10 times more resistant than the binding of CvMab-62 to the trimeric BQ.1 ectodomains. This implies that, in regard to the binding with Bis-Beb and the BQ.1 spike, not only CvMab-62's Fab but also bebtelovimab's scFv contributes to the observed effect. As the BQ.1 variant is resistant to bebtelovimab, ELISA was conducted to investigate whether Bis-Beb inhibits the binding between the ACE2 and trimeric BQ.1.1 ectodomain (Figure 8C). The results showed that both the original bebtelovimab and CvMab-62, even at a concentration of 10 μg/mL, were unable to inhibit the binding between the ACE2 and BQ.1.1 RBD in the trimeric spike ectodomain. In contrast, Bis-Beb significantly inhibited binding between the ACE2 and BQ.1.1 RBD in the trimeric spike ectodomain (Figure 8C; red bar). These results suggest that both CvMab-62's Fab and bebtelovimab's scFv contributes to the binding between Bis-Beb and the trimeric BQ.1 spike ectodomain.

Next, we evaluated antiviral activity against BQ.1-type viruses. When testing the BA.5.2 pseudotyped virus, both bebtelovimab and Bis-Beb displayed similar low IC_{50} values (Figure 8D, open circles and open squares, respectively). However, when confronted with the BA.5.2 pseudotyped virus carrying the K444T mutation, a known factor in bebtelovimab resistance,[26,30,31] Bis-Beb exhibited an approximately 100-fold lower IC_{50} value compared to bebtelovimab (Figure 8D; blue circles and red squares, respectively). These findings suggest that Bis-Beb effectively overcomes resistance caused by the K444T mutation.

This inhibitory effect was further confirmed using live viral infection experiments (Figure 8E). When VeroE6/TMPRSS2 cells were infected with BA.5.21 (TY41-721), Bis-Beb demonstrated a low IC_{50} value similar to that of bebtelovimab. Conversely, for BQ.1.1 (TY41-796) infection, bebtelovimab proved ineffective, whereas Bis-Beb exhibited infection-inhibitory activity with 2.6 nM IC_{50} values (Figure 8E; red symbols).

Bispecific antibodies Bis3 and Bis-Beb are based on the mouse-derived anti-S2 antibody CvMab-62, which is not suitable for therapeutics, therefore, we have created humanized Bis-Beb and CvMab-62. ELISA experiments indicated that *in vitro* binding of humanized Bis-Beb to the

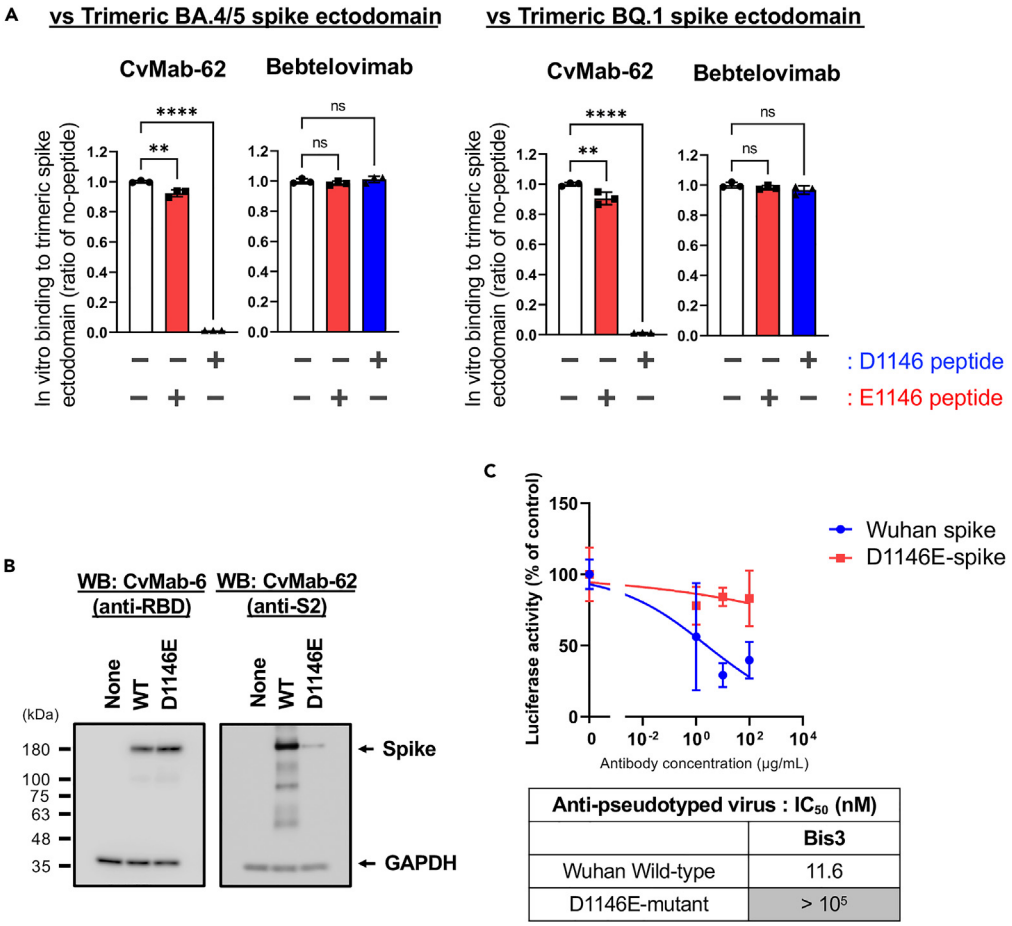

Anti-pseudotyped virus : IC_{50} (nM)	
	Bis3
Wuhan Wild-type	11.6
D1146E-mutant	> 10^5

Figure 4. Binding by CvMab-62 is critical for neutralizing activity of bispecific antibody

(A) *In vitro* binding of CvMab-62 to the trimeric spike was inhibited by the novel S2 epitope. *In vitro* binding of CvMab-62 to the trimeric spike ectodomain, was measured using ELISA. CvMab-62 was preincubated with 1 μM of epitope peptide (D1146) or D1146E mutated peptide (E1146), and subsequently added to the trimeric spike ectodomain protein coated ELISA plate. Data are presented as the means ± SD (n = 3). Statistical differences were determined using a one-way analysis of variance (ANOVA), and a p value <0.05 was considered statistically significant, **p < 0.01, and ****p < 0.0001. ns was not statistically significant.

(B) Western blotting analysis of D1146E mutated spike protein. Spike proteins of Whuan-Hu-1 and D1146E mutants were expressed in HEK293T cells and detected using CvMab-6 or CvMab-62 antibodies.

(C) Neutralization activity of Bis3 against the D1146E-mutanted spike-expressing pseudotyped virus. Wuhan wild-type or D1146E-mutated spike-expressing pseudotyped viruses were preincubated with Bis3 at the indicated concentrations and they were then used to infect VeroE6/TMPRSS2 cells. Three days post-infection, cellular luciferase activity was measured to estimate the pseudotyped virus infection ratio. Data are presented as the means ± SD (n = 3).

trimeric Wuhan spike ectodomain was at the same level as that of the mouse-derived Bis-Beb, whereas that of humanized CvMab-62 was apparently weaker than that of mouse CvMab-62 (Figure 9A). Moreover, we found that humanized Bis-Beb showed stronger binding to the trimeric BQ.1 spike ectodomain than did bebtelovimab and humanized CvMab-62 (Figure 9B). Next, the neutralizing activity of humanized Bis-Beb was also tested in the K444T-mutated BA.5.2 pseudoyped virus and BQ.1.1 live virus. Similar to the original mouse-derived Bis-Beb (Figure 8), humanized Bis-Beb exhibited lower IC_{50} values than bebtelovimab (Figures 9C and 9D). These findings suggest that Bis-Beb effectively overcomes the resistance caused by the K444T mutation. Taken together, these results suggest that Bis-Beb restores the inhibitory effect on binding between the RBD of BQ.1.1 and ACE2, thereby inhibiting infection with BQ.1.1 (Figure 9E).

DISCUSSION

In this study, we generated neutralizing bispecific antibodies in the IgG-scFv format by combining ineffective anti-RBD antibodies with anti-S2 antibody, which is a new and distinct structure from previous studies. Notably, the epitope targeted by the anti-S2 antibody in this study was a novel location near the known epitope of anti-S2 antibodies. Furthermore, the structure of the bispecific antibodies, simple fusion of the scFv of the anti-RBD antibody with the C-terminus of the heavy chain of the anti-S2 antibody, can enhance neutralization activity. Moreover, by applying this basic structure, we created bispecific antibodies by combining the scFv of bebtelovimab with our anti-S2 antibody, demonstrating partial overcoming of the resistance to BQ.1.1. This suggests that neutralizing bispecific antibodies, combining existing therapeutic

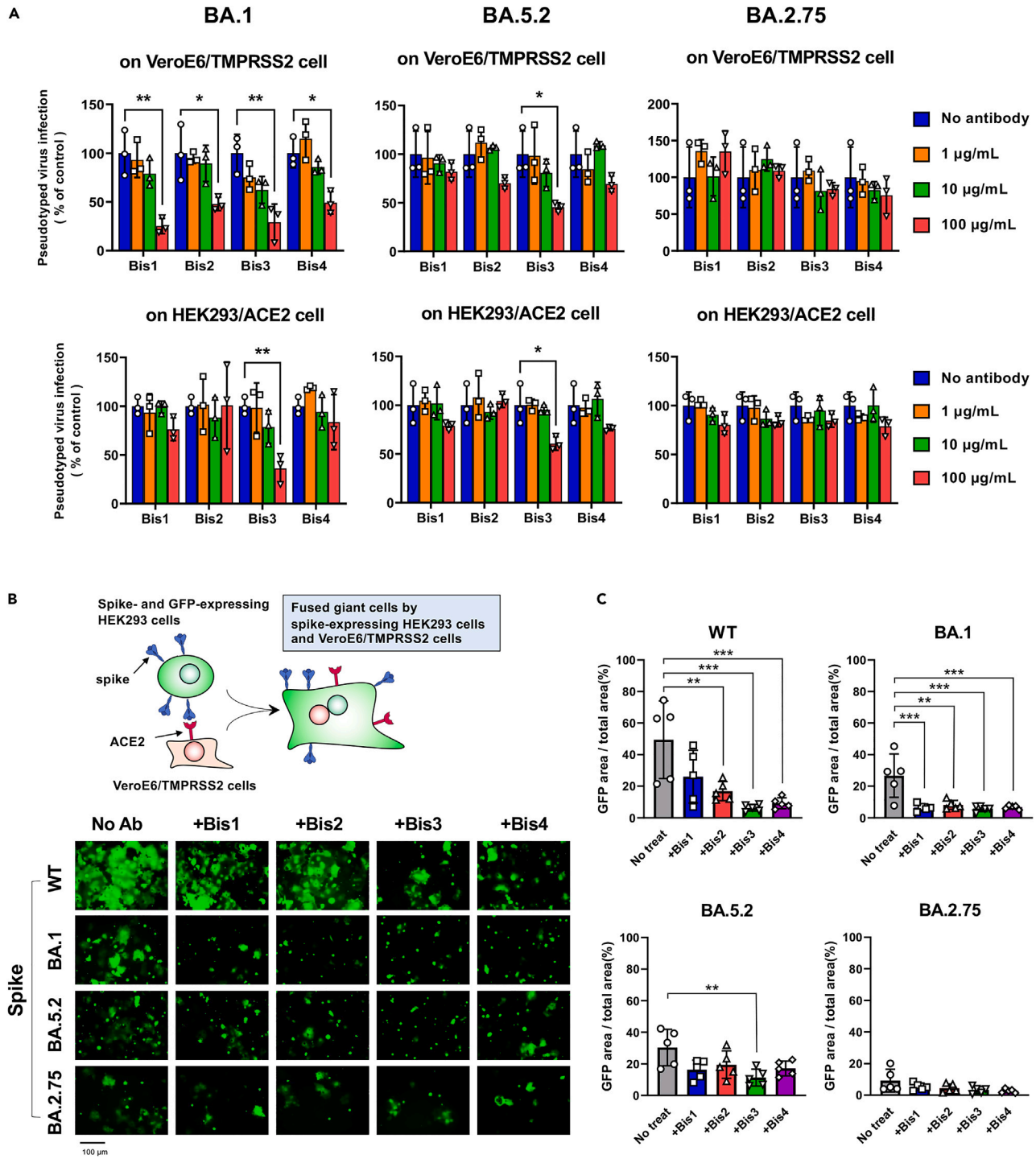

Figure 5. Bis3 suppresses endocytosis-mediated pseudotyped virus infection and spike-mediated cell-cell fusion

(A) Omicron-type SARS-CoV-2 pseudotyped viruses were preincubated with bispecific antibodies at the indicated concentrations and then used to infect VeroE6/TMPRSS2 or HEK293/ACE2 cells. The infection rate was monitored by measuring the luciferase activity of the pseudovirus reporter. Data are presented as the means ± SD (n = 3). Statistical significance was set at a p value <0.05, and one-way ANOVA was employed, *p < 0.05, **p < 0.01.

(B) Schematics of the cell-cell fusion assay are presented in the upper section. Spike- and GFP-transfected HEK293 cells were suspended, preincubated with bispecific antibodies, and overlaid onto a monolayer of VeroE6/TMPRSS2 cells. After 3 h, the GFP-positive fused cells were photographed (lower panels).

(C) The green signal area of GFP-positive fused cells, as in B, was quantified using ImageJ, and the results are shown as a bar graph. Data are presented as the means ± SD (n = 5). Statistical significance was considered at a p value <0.05, and one-way ANOVA was employed; **p < 0.01, ***p < 0.001.

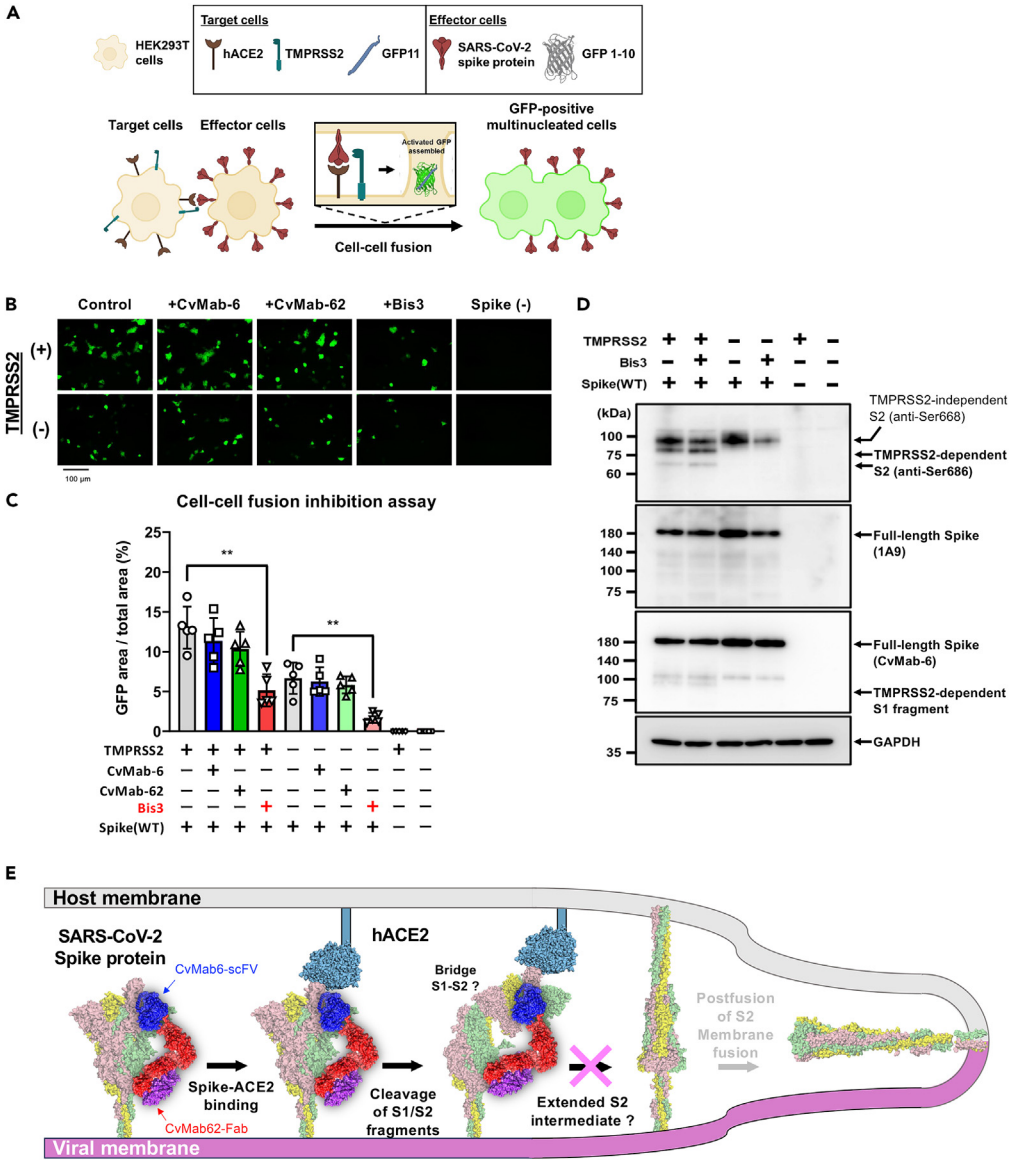

Figure 6. Inhibition of cell-cell fusion by bispecific antibody is independent of S2 cleavage by TMPRSS2

(A) Schematics of the cell-cell fusion assay with a split GFP system are presented. As target cells, HEK293T cells were transfected with ACE2, TMPRSS2 and split GFP11. As effector cells, SARS-CoV-2 spikes and split GFP 1–10 were co-transfected into HEK293T cells. When both cell types were mixed to generate fused cells, reconstituted GFP signals were detected.

(B) Wuhan-type spike-expressing effector cells were suspended, preincubated with parental CvMab-6, CvMab-62 or bispecific Bis3 antibodies, and overlaid onto a monolayer of target cells. After 3 h, the GFP-positive fused cells were photographed (upper panels).

(C) The green signal area of GFP-positive fused cells, as in B, was quantified using ImageJ, and the results are shown as a bar graph. Data are presented as the means ± SD (n = 5). Statistical significance was considered at a p value <0.05, and one-way ANOVA was employed; **p < 0.01.

(D) After cell fusion by target and effector cells, as in B, S2 cleavage in effector cells was examined by western blot analysis probed with an anti-Ser 686 S2 antibody. TMPRSS2-dependent S2 cleavage was detected and was not affected by bispecific antibody preincubation.

(E) Hypothesis of the mechanism of action of the bispecific antibody Bis3. The bispecific antibody Bis3 binds to both the RBD and S2 domains of the spike protein without inhibiting S1/S2 cleavage. Consequently, Bis3 may interfere with the intermediate steps that occur between detachment of the S1 segment and the subsequent membrane fusion process involving the postfusion form of the S2 component.

antibodies with S2 antibodies, can revive the value of anti-RBD antibody therapeutics which have diminished in utility owing to resistance issues. Consequently, this approach represents a promising strategy for overcoming antibody therapeutic resistance issues and is worthy of consideration.

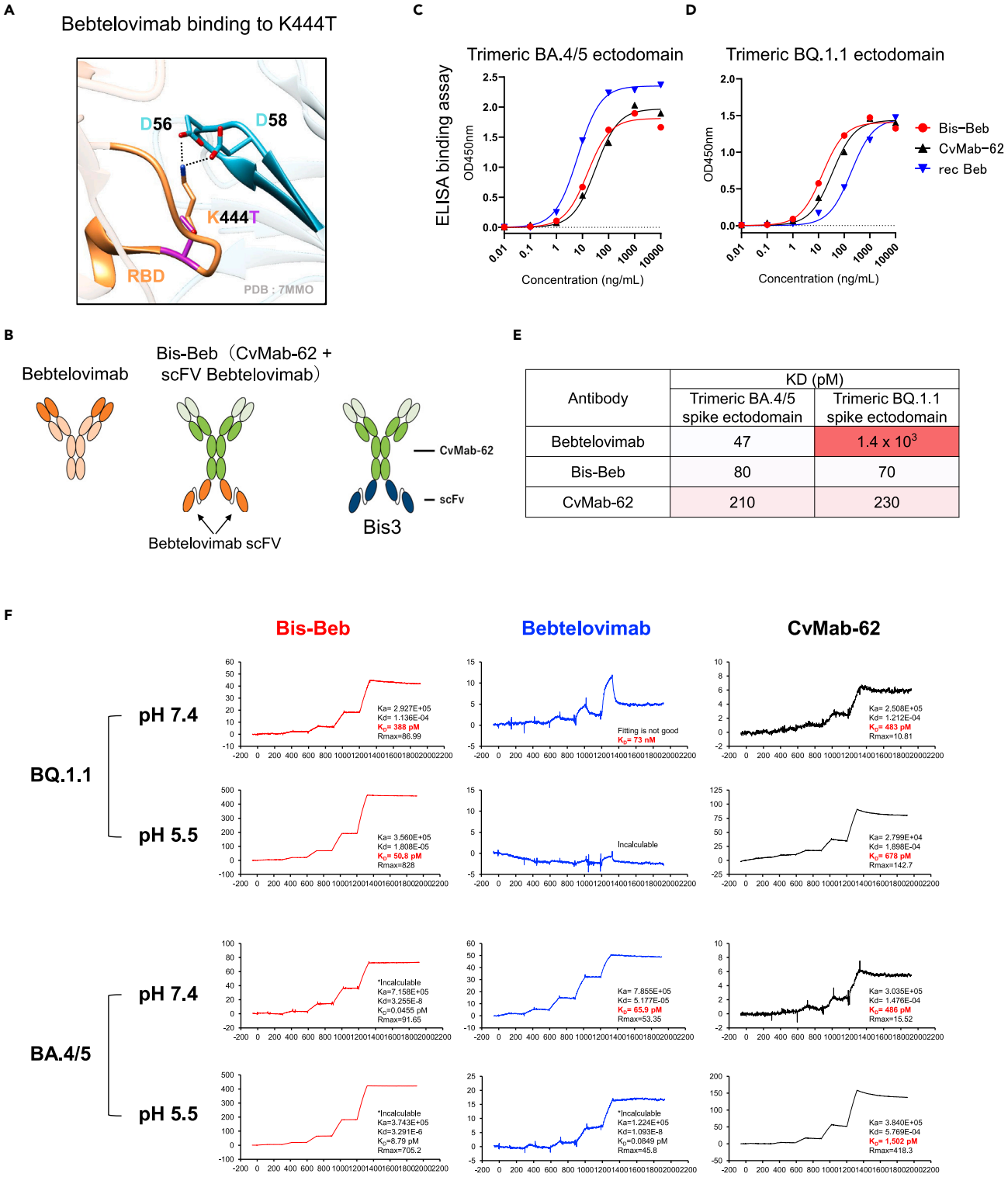

Antibody	KD (pM)	
	Trimeric BA.4/5 spike ectodomain	Trimeric BQ.1.1 spike ectodomain
Bebtelovimab	47	1.4×10^3
Bis-Beb	80	70
CvMab-62	210	230

Figure 7. Bispecific antibody constructed with bebtelovimab and CvMab-62

(A) Structural model of bebtelovimab CDR binding to SARS-CoV-2 RBD. The K444 residue in the RBD of the SARS-CoV-2 spike protein interacts with D185 and D187 in the heavy-chain CDR of bebtelovimab. The BQ.1.1 variant of the spike protein has a mutation at K444 (replaced by T), which is responsible for making it resistant to bebtelovimab.

(B) Schematic of the bispecific antibody Bis-Beb. The scFv of anti-RBD bebtelovimab was fused with the C-terminus of the anti-S2 CvMab-62 heavy chains.

Figure 7. *Continued*

(C) *In vitro* binding of the bispecific antibody to trimeric spike ectodomain of omicron BA.4/5 consisting of 1231 amino acids measured by ELISA.

(D) *In vitro* binding of the bispecific antibody to the trimeric spike ectodomain of Omicron BQ.1.1, consisting of 1231 amino acids, as measured by ELISA. The wells were coated with the trimeric spike ectodomain protein, and bispecific antibodies at the indicated concentrations were added to evaluate antibody binding to the trimeric spike protein.

(E) Summary table of the *in vitro* binding ability of the bispecific antibody in ELISA. The KD values were estimated using C and D by GraphPad Prism9.

(F) SPR analysis of the bispecific antibody against the trimeric spike ectodomain. The spike ectodomain, either BQ.1.1 or BA. 4/5 was captured as a ligand, and two buffer conditions, pH 7.4 and pH 5.5, were tested. Antibody as an analyte, Bis-Beb (red lines), bebtelovimab (blue lines), and CvMab-62 (black lines) were tested. The response curves are representative of the two experiments. *The reported kinetic constant kd was outside the limits measured using the instrument in this study.

Numerous antiviral antibodies with inhibitory activity against SARS-CoV-2 infection have been developed, and some have been applied in clinical settings.[4,6,57] While all anti-SARS-CoV-2 antibody therapeutics target the RBD, newly emerged variants have immune-evasive mutations, particularly within the RBD. Consequently, the clinical application of anti-RBD antibodies has led to reduced neutralization and inhibitory activities.[22,26,30,31,58] Although efforts to develop broadly neutralizing antibodies that target pan-coronavirus conserved epitopes are actively underway,[59–66] the possibility of emerging immune-evading mutant variants remains, posing a recurrent challenge to monoclonal antibody therapy. Therefore, the exploration of alternative approaches is attractive. Another approach is to investigate different antibody formats, bispecific or multispecific, that can simultaneously and synergistically bind to multiple epitopes.[42–44,67–74]

A study on bispecific antibodies combining anti-RBD and anti-S2 antibodies has been reported.[44] The structure of these bispecific antibodies involved a combination of scFvs from neutralizing antibodies against RBD and S2, arranged in tandem in the scFv-scFv-Fc format. Unfortunately, the specific epitope targeted by the anti-S2 antibodies has not yet been described. These bispecific antibodies did not show significant improvement in blocking the binding between the RBD and ACE2 compared with the monoclonal antibodies from which they originated. However, their infection-inhibitory activity against mutant variants was enhanced by bispecific antibody formation. This suggests that developing bispecific antibodies targeting both the RBD and S2 is an effective approach for creating broad-spectrum neutralizing antibodies against mutant variants.

Unlike anti-RBD neutralizing antibodies, the infection-inhibitory mechanism of anti-S2 antibodies does not involve the inhibition of binding between ACE2 and RBD; thus, another neutralizing mechanism is involved. The S2 region of the spike protein undergoes significant structural changes between prefusion and postfusion states.[75,76] A similar phenomenon in the S2 region has been proposed for the MERS-CoV spike protein.[77,78] During the transition from the prefusion to the postfusion form, there is a substantial structural alteration in the linker region between subdomain (SD)3 and hepta-repeat (HR)2, and it is suggested that the correct refolding of this linker region is crucial for forming the central HR1–HR2 six-helix bundle. This bundle brings the viral membrane closer to the host membrane during the late stages of fusion transition.[77] Dynamic structural changes in the S2 region of SARS-CoV-2 have been observed during membrane fusion and intermediate structures have been elucidated.[79] Specifically, a model was proposed in which the S2 region was extended, sandwiching the SD3 region between HR1 and HR2, allowing it to fold back and form a postfusion six-helical bundle. Notably, many anti-S2 antibodies targeting SARS-CoV-2 have been reported to exhibit infection inhibitory activity, with several antibodies binding upstream of HR2, the S2 stem helix region within residues 1141–1160 of the spike protein.[34,36–38,40,41,47,80] The alpha helix within residues 1148–1156 (FKEELDKYF) upstream of HR2 is a common epitope for most anti-S2 neutralizing antibodies, and residues F1148, E1151, L1152, D1153, Y1151, and F1156 are directly recognized by the anti-S2 antibody S2P6 complementarity-determining regions (CDRs).[34,47] In particular, as suggested by the S2P6 model,[34] anti-S2 antibodies inhibit the structural conversion of the S2 region necessary for cellular membrane fusion.

Regarding the anti-S2 antibody CvMab-62 epitope, Figure 2 shows that CvMab-62 binding to the S2 region does not require residues 1149–1162 (KEELDKYFKNHTSP); however, the D1146E mutation abolished CvMab-62 binding to S2. Hence, it was inferred that the binding mechanism of CvMab-62 differs from that of typical S2 antibodies, primarily because it does not depend on the epitopes commonly required by anti-S2 neutralizing antibodies, and the orientation of residue D1146, which is essential for CvMab-62 binding, is on the opposite side to where S2P6 binds (Figure S5).[34,47] These data suggest that binding to the novel S2 epitope is crucial for the inhibitory activity of the bispecific antibody Bis3 (Figure 4), and a structural analysis of the binding mode is necessary.

On the contrary, a search of the GISAID database (November 30, 2023), identified 543 cases of the D1146E mutation among 16,270,655 viral genomes (frequency approximately 0.0033%). Considering that viruses harboring the D1146E mutation have been detected in the presently circulating XBB lineage, and the XBB variants with the V445P mutation exhibit resistance to Bis-Beb (Figure S6), it raises the possibility that the utilization of the bispecific antibody based on CvMab-62 could still permit the survival of the escape variants. Furthermore, a recent study has suggested that the spike protein of the bat sarbecovirus Khosta2, not recognized by CvMab-62, holds the potential to infect humans.[81] Consequently, spillover events of Khosta2-like sarbecoviruses from bats to humans might lead to the evasion of CvMab-62-based bispecific antibodies.

In addition, the bispecific antibody Bis3 did not significantly interfere with the TMPRSS2-dependent spike protein cleavage into the S2 fragment. Therefore, it is presumed that CvMab-62 inhibits the fusion process between the virus and the cell membrane after proteolytic cleavage of the spike protein. Interestingly, the anti-SARS-CoV-2 neutralizing antibody SP1-77 inhibits S1 fragment dissociation from the pre-cleaved S1/S2 complex, thereby blocking the activation of the fusion peptide and membrane fusion.[82] The bispecific antibody Bis3 might potentially obstruct the structural changes in S2 as S1 separates or create steric hindrance against S1 fragment dissociation from the pre-cleaved S1/S2 complex due to dual binding between the RBD and S2 regions (Figures 6E and 9E).

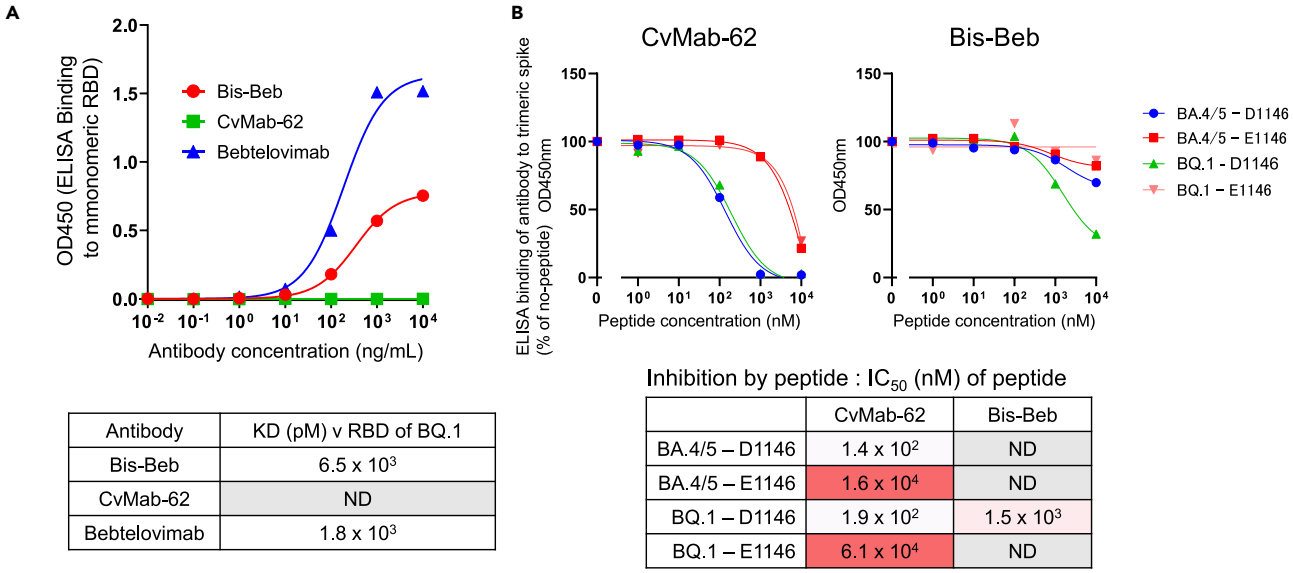

Antibody	KD (pM) v RBD of BQ.1
Bis-Beb	6.5 x 10^3
CvMab-62	ND
Bebtelovimab	1.8 x 10^3

Inhibition by peptide : IC_{50} (nM) of peptide

	CvMab-62	Bis-Beb
BA.4/5 – D1146	1.4 x 10^2	ND
BA.4/5 – E1146	1.6 x 10^4	ND
BQ.1 – D1146	1.9 x 10^2	1.5 x 10^3
BQ.1 – E1146	6.1 x 10^4	ND

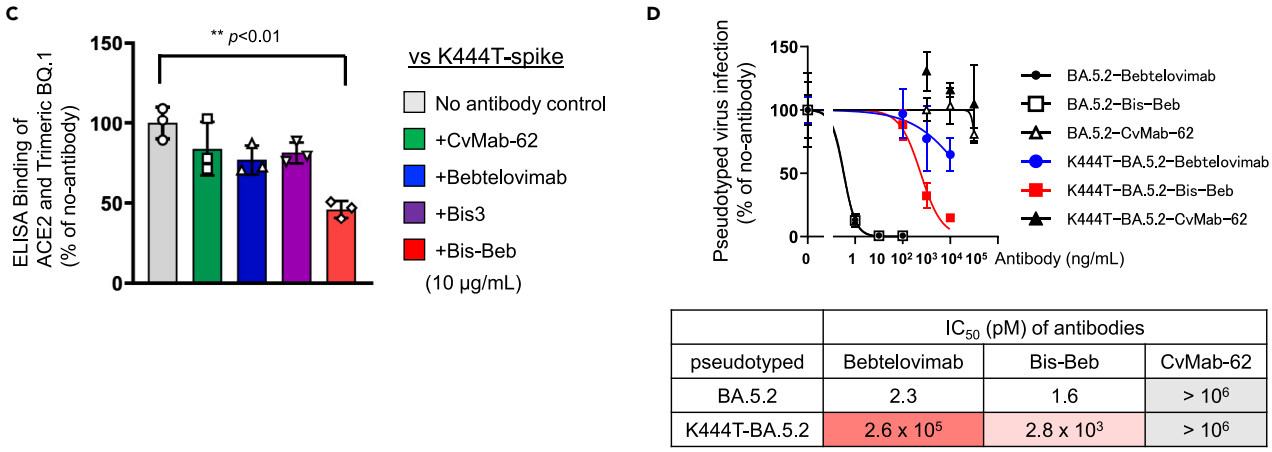

	IC_{50} (pM) of antibodies		
pseudotyped	Bebtelovimab	Bis-Beb	CvMab-62
BA.5.2	2.3	1.6	> 10^6
K444T-BA.5.2	2.6 x 10^5	2.8 x 10^3	> 10^6

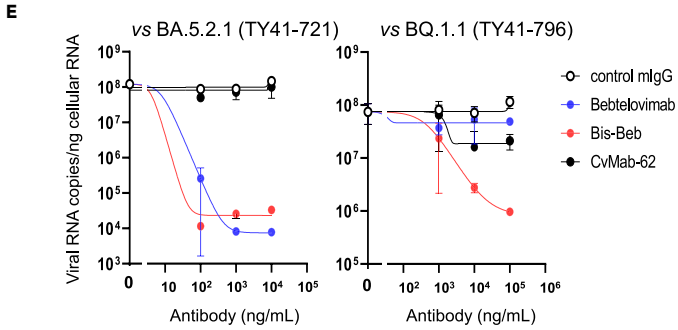

	IC_{50} (pM) of antibodies		
Live virus	Bebtelovimab	Bis-Beb	CvMab-62
BA.5.2.1	54	20	> 10^3
BQ.1.1	> 10^6	2.6 x 10^3	> 10^4

Figure 8. Neutralizing ability of Bis-Beb against bebtelovimab-resistant BQ.1.1

(A) *In vitro* binding of the bispecific antibody to the monomeric RBD of BQ.1, was measured using ELISA. The wells were coated with the monomeric BQ.1 RBD protein, and antibodies at the indicated concentrations were added to evaluate antibody binding. The KD values estimated by GraphPad Prism9 are summarized in the table below.

(B) Relative resistance to *in vitro* binding of Bis-Beb to the trimeric spike. *In vitro* binding of CvMab-62 or Bis-Beb to the trimeric spike ectodomain, was measured using ELISA. Antibodies were preincubated with the epitope peptide (D1146) or D1146E mutated peptide (E1146) at the indicated concentrations, and subsequently added to a trimeric spike ectodomain protein-coated ELISA plate.

Figure 8. *Continued*

(C) Inhibition of *in vitro* ACE2-spike binding by the bispecific antibody was confirmed using ELISA. His-tagged trimeric spike ectodomain of BQ.1.1 was preincubated with bispecific antibodies (10 μg/mL), and then premixtures added to a well coated with recombinant ACE2 protein. After washing, the ACE2-bound trimeric spike protein was probed with anti-His-tag antibodies. Data are presented as the means ± SD (n = 3).

(D) Neutralization of bispecific antibodies against SARS-CoV-2 pseudotyped viruses. Pseudotyped viruses (expressing BA.5.2- or K444T mutated BA.5.2-type spike) were preincubated with antibodies at the indicated concentrations and then used to infect VeroE6/TMPRSS2 cells. Three days post-infection, cellular luciferase activity was measured to estimate the pseudotyped virus infection ratio. Data are presented as the means ± SD (n = 3). The inhibitory effects of bispecific antibodies are shown as IC_{50} values and summarized in the table below.

(E) Neutralization of bispecific antibodies against authentic SARS-CoV-2. Authentic SARS-CoV-2 variants (BA.5.2.1 or BQ.1.1) were preincubated with antibodies at the indicated concentrations and then used to infect VeroE6/TMPRSS2 cells. At 24 h post-infection, viral genomic RNA in the cells was measured by quantitative RT-PCR, and viral replication shown as the ratio of the control. Data are presented as the means ± SD (n = 4). The inhibitory effects of bispecific antibodies are shown as IC_{50} values and summarized in the table below.

Bis3 was effective in neutralizing the Omicron variants BA.1 and BA.5.2, particularly by blocking infection through the endosomal pathway. Although CvMab-62 and CvMab-6 appeared to interact equally with the spike proteins of BA.1, BA.5.2, and BA2.75, Bis3 was not effective against BA.2.75, although it is believed to use a similar infection pathway. Previous studies have suggested that the RBD of BA.2.75 binds more strongly to its receptor ACE2 than BA.5.[83] Additionally, the BA.2.75 spike protein exhibits decreased thermostability and a higher frequency of the RBD being in the "up" conformation under acidic conditions, which suggests enhanced cell entry at low pH through the endosomal pathway.[84] These robust infectious characteristics may explain why Bis3 was unable to inhibit infection with BA.2.75. Another possibility is that the Bis3-inhibiting mechanism is a fusogenic process involving the spike protein. Previous studies and our data indicate that the Omicron spike protein has low fusogenic activity.[48,50,84] The fusogenic activity of BA.2.75 may play only a small role in its infection process; hence, BA.2.75 spike-mediated infection may be unaffected by Bis3. Recent studies have suggested that SARS-CoV-2 cell entry is instigated by clathrin-mediated endocytosis or Rac1-, Cdc42-, and Pak1-mediated macropinocytosis.[85,86] SARS-CoV-2 entry and viral spike-mediated cell-cell fusion mechanisms may rely on different signaling pathways for initiation, and the BA.2.75-spike mediated viral entry mechanism may differ from the Bis3-sensitive cell-cell fusion mechanism. Further investigation is required to confirm these observations.

Bebtelovimab is classified as a class 3 anti-RBD antibody.[29] Notably, the epitope targeted by bebtelovimab is conserved among many SARS-CoV-2 variants. It has shown efficacy against various mutant variants; however, it has lost its effectiveness against recent variants, such as BQ.1.1 and XBB.1.5.[26,27,30] Specifically, a significant contributor to bebtelovimab resistance in BQ.1.1 is the K444T mutation.[29] It is presumed that this amino acid mutation interferes with the binding between bebtelovimab and RBD. Further, SPR analysis revealed that bebtelovimab exhibits weak binding and rapid dissociation from BQ.1.1, particularly under acidic conditions such as those found in the endosome, where bebtelovimab fails to bind to the BQ.1.1 spike protein (Figure 7F). Bis-Beb, similar to its parent antibody CvMab-62, maintained stable binding to BQ.1.1, even under acidic conditions. Although bebtelovimab alone cannot inhibit the binding between the RBD of BQ.1.1 and ACE2, its ability to block this interaction is crucially restored when incorporated into the bispecific antibody. Our observations suggested that the scFv derived from bebtelovimab is more likely to be in close proximity to the RBD in a bispecific format. This, in turn, may block the binding between the RBD and ACE2.

Taken together, the bispecific antibody, Bis-Beb, generated in our study, exhibited a remarkable capability to restore neutralization activity against the bebtelovimab-resistant variant BQ.1.1. It should be noted that Bis-Beb in our study apparently overcame the resistance conferred by the K444T mutation in BQ.1.1. However, Bis-Beb is not a universal anti-resistance bispecific antibody. The primary reason for bebtelovimab resistance in XBB.1.5 is the V445P mutation, and we did not observe significant overcoming of V445P-mediated resistance by Bis-Beb (Figure S6). Hence, to overcome bebtelovimab resistance in XBB.1.5, alternative strategies are required, and it is important to explore the various structural configurations and combinations of antibodies to identify effective bispecific antibodies. In addition, the antibody-mediated Fc effector functions such as antibody dependent cellular cytotoxicity (ADCC) are important components of immunological protection.[87–89] Unfortunately, ADCC activity was not detected withe the current IgG-scFv bispecific antibodies Bis-Beb (Figure S7). Furthermore, there are concerns regarding *in vivo* efficacy of the IgG-scFv formatted bispecific antibody. Several previous studies have reported challenges related to the *in vivo* stability of bispecific antibodies. In the case of bispecific antibodies, in which scFv is fused to the C-terminus of the Fc region of IgG, a shortened half-life in the bloodstream has been observed.[90,91] This phenomenon can be attributed to a reduction in FcRn binding, possibly resulting from the steric hindrance caused by the attached scFv.

Thus, in future research, modifications to the Fc portion of bispecific antibodies should be introduced in order to enhance ADCC activity and blood persistence, and this enhancement is integral for improving *in vivo* efficacy of bispecific antibodies. Although Fc-dependent antibody responses could demonstrate antiviral benefits when properly regulated, they may contribute to immunopathology when dysregulated. Therefore, balancing the benefits and safety considerations will be essential for further development of more effective broad-spectrum bispecific neutralizing antibodies.

Limitations of the study

This study showed that bispecific antibodies constructed using non-neutralizing anti-RBD and anti-S2 antibodies with different epitopes can gain neutralizing activity against antibody-resistant SARS-CoV-2 variants. We analyzed the biochemical characteristics of bispecific antibodies using an *in vitro* assay. However, the bispecific antibodies described here have limited potency because a high concentration of Bis3 and a relatively high concentration of Bis-Beb were needed for the SARS-CoV-2 neutralization, and mouse antibodies were not suitable for use in human therapy. Second, the structural characteristics of CvMab-62 binding to its epitope near the S2 stem helix remain unknown. A three-dimensional structural analysis is required to clarify the molecular mechanism of CvMab-62 binding to the S2 epitope.

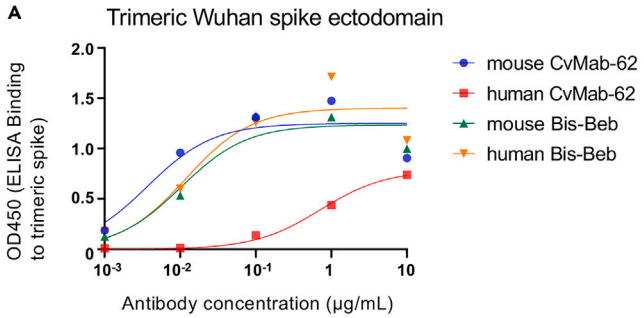

Antibody	K_D (pM) vs Wuhan trimeric spike
mouse CvMab-62	24
humanized CvMab-62	4.6 x 10^3
mouse Bis-Beb	49
humanized Bis-Beb	59

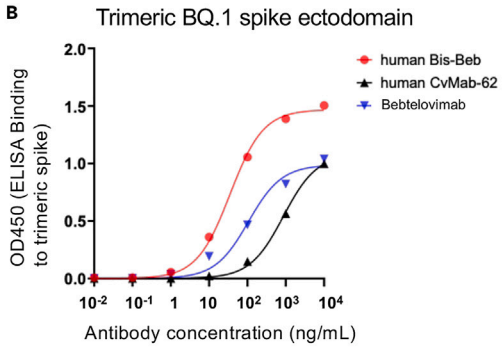

Antibody	K_D (pM) vs BQ.1 trimeric spike
humanized CvMab-62	6.2 x 10^3
humanized Bis-Beb	160
Bebtelovimab	780

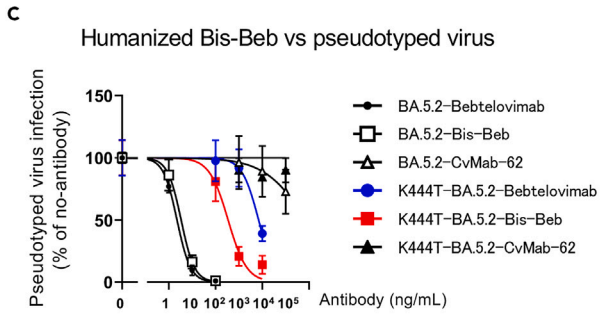

	IC_{50} (pM) of antibodies		
	Bebtelovimab	humanized Bis-Beb	humanized CvMab-62
BA.5.2	15.6	16.4	> 10^5
K444T-BA.5.2	4.8 x 10^4	1.7 x 10^3	> 10^5

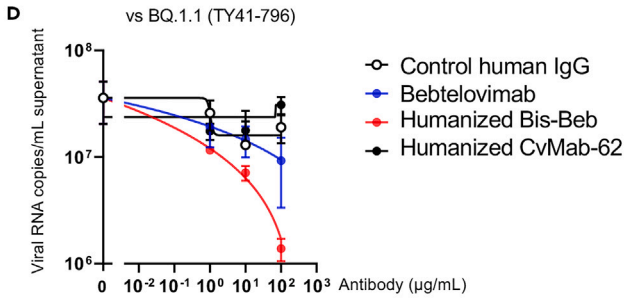

Antibody	IC_{50} (pM) of antibodies
humanized CvMab-62	ND
humanized Bis-Beb	4.7 x 10^2
Bebtelovimab	4.9 x 10^4

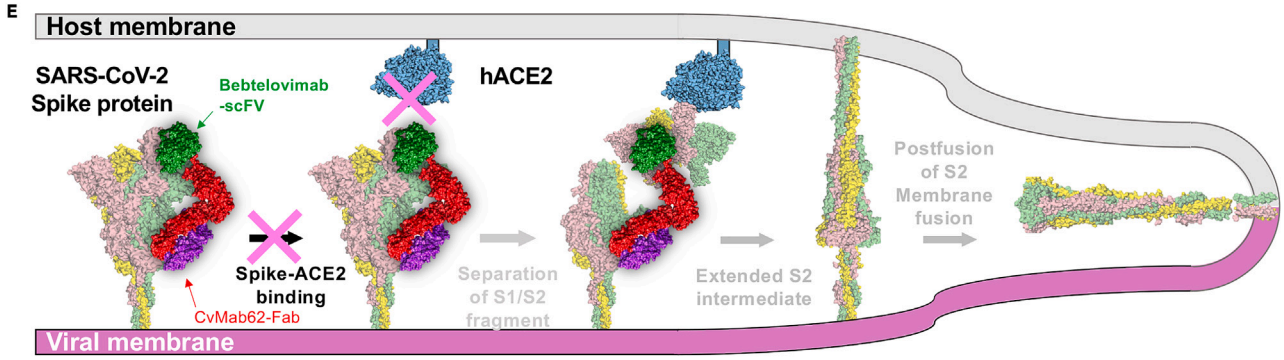

Figure 9. Neutralizing ability of humanized Bis-Beb against bebtelovimab-resistant BQ.1.1

(A) *In vitro* bindings of the mouse-derived and humanized antibodies to the trimeric spike ectodomain of the Wuhan type was compared using ELISA. The calculated KD values using GraphPad Prism9 are presented in the table below.

(B) *In vitro* binding of the mouse-derived and humanized antibodies to monomeric RBD or trimeric spike ectodomain proteins was measured by ELISA. The BQ.1 monomeric RBD or trimeric ectodomain proteins were coated in the wells, and antibodies at the indicated concentrations were added. The calculated KD values using GraphPad Prism9 are presented in the table below.

Figure 9. *Continued*

(C) Neutralization of humanized bispecific antibodies against SARS-CoV-2 pseudotyped viruses. Pseudotyped viruses (expressing BA.5.2- or K444T mutated BA.5.2-type spike) were preincubated with antibodies at the indicated concentrations and they were then used to infect VeroE6/TMPRSS2 cells. Three days post-infection, cellular luciferase activity was measured to estimate the pseudotyped virus infection ratio. Data are presented as the means ± SD (n = 3). The inhibitory effects of the bispecific antibodies are shown as IC_{50} values and are summarized in the table below.

(D) Neutralization of humanized bispecific antibodies against SARS-CoV-2. Authentic SARS-CoV-2 variants (BA.5.2.1 or BQ.1.1) were preincubated with antibodies at the indicated concentrations and used to infect VeroE6/TMPRSS2 cells. At 24 h post-infection, viral RNA in the medium supernatant was measured by quantitative RT-PCR, and viral replication was calculated as the ratio of the control. Data are presented as the means ± SD (n = 4). The inhibitory effects of the bispecific antibodies are shown as IC_{50} values and are summarized in the table below. The ND was not determined.

(E) Mechanism of action of the bispecific antibody Bis-Beb. Bis-Beb binds to the RBD and S2 domains of the spike protein. Bis-Beb can restore the ability to inhibit binding between BQ.1.1 RBD and ACE2 and has the capacity to interfere with the subsequent membrane fusion process involving the postfusion form of the S2 component.

Finally, animal model experiments to evaluate the *in vivo* safety and efficacy of these novel bispecific antibodies have not been performed. Therefore, humanized bispecific antibodies with enhanced ADCC activity should be developed to determine their pharmaceutical mechanisms *in vitro* and *in vivo*.

STAR★METHODS

Detailed methods are provided in the online version of this paper and include the following:

- KEY RESOURCES TABLE
- RESOURCE AVAILABILITY
  - Lead contact
  - Materials availability
  - Data and code availability
- EXPERIMENTAL MODEL AND STUDY PARTICIPANT DETAILS
  - Animals for hybridoma production
  - Cell culture
  - SARS-CoV-2 viruses
- METHOD DETAILS
  - Spike plasmid construction
  - Development of bispecific antibody
  - ELISA for antibody development
  - CvMab-6 epitope mapping
  - CvMab-62 epitope mapping
  - Pseudotyped virus neutralization assay
  - Authentic SARS-CoV-2 neutralization assay
  - Quantification of viral RNA
  - Immunoblotting
  - Immunofluorescence microscopic analysis
  - Cell-cell fusion assay
  - ELISA for binding affinity calculation
  - ELISA for *in vitro* RBD and ACE2 neutralization assay
  - The surface plasmon resonance (SPR) experiments
  - Structural modeling of the spike protein
  - Antibody-dependent cellular cytotoxicity (ADCC) assay
- QUANTITATIVE AND STATISTICAL ANALYSIS

SUPPLEMENTAL INFORMATION

Supplemental information can be found online at https://doi.org/10.1016/j.isci.2024.109363.

ACKNOWLEDGMENTS

This research was supported in part by an on-campus grant in TUS, funded by donations from "Account for Donations to Develop Vaccine and Medicine to Treat COVID-19" established by the Sumitomo Mitsui Trust Bank (K.N), JSPS KAKENHI JP22K15284 (Y.Y), and by Japan Agency for Medical Research and Development under Grant Numbers: 21fk0108568h0001 (Y.Y. and K.N.), 21fk0108568j0101 (M.F), 21wm0325032s0101 (K.N.), 21wm0325032j0201 (M.F.), JP23ama121008 (Y.K.), JP23a.m.0401013 (Y.K.), 23bm1123027h0001 (Y.K.), JP23ck0106730 (Y.K.), and JP21a.m.0101078 (Y.K.). We thank Editage (www.editage.jp) for English language editing.

AUTHOR CONTRIBUTIONS

Conceptualization, Y.K. and K.N.; investigation, T.I., Y.Y., K.S., Y.N., Y.S., M.O., M.K., and K.N.; resources, M.F., T.O., Y.T., and T.W.; writing–original draft preparation, T.I., Y.N., Y.S., M.F., Y.K., and K.N.; writing–review and editing, M. F., Y.K., and K.N.; funding acquisition, Y.Y., M.F., Y.K., and K.N. All authors discussed the results and commented on the manuscript.

DECLARATION OF INTERESTS

The authors declare no competing interests related to the present manuscript.

Received: October 27, 2023
Revised: January 22, 2024
Accepted: February 26, 2024
Published: February 29, 2024

REFERENCES

1. Li, G., Hilgenfeld, R., Whitley, R., and De Clercq, E. (2023). Therapeutic strategies for COVID-19: progress and lessons learned. Nat. Rev. Drug Discov. *22*, 449–475. https://doi.org/10.1038/s41573-023-00672-y.
2. Gupta, A., Gonzalez-Rojas, Y., Juarez, E., Crespo Casal, M., Moya, J., Falci, D.R., Sarkis, E., Solis, J., Zheng, H., Scott, N., et al. (2021). Early Treatment for Covid-19 with SARS-CoV-2 Neutralizing Antibody Sotrovimab. N. Engl. J. Med. *385*, 1941–1950. https://doi.org/10.1056/NEJMoa2107934.
3. Self, W.H., Sandkovsky, U., Reilly, C.S., Vock, D.M., Gottlieb, R.L., Mack, M., Golden, K., Dishner, E., Vekstein, A., Ko, E.R., et al. (2022). Efficacy and safety of two neutralising monoclonal antibody therapies, sotrovimab and BRII-196 plus BRII-198, for adults hospitalised with COVID-19 (TICO): a randomised controlled trial. Lancet Infect. Dis. *22*, 622–635. https://doi.org/10.1016/S1473-3099(21)00751-9.
4. Taylor, P.C., Adams, A.C., Hufford, M.M., de la Torre, I., Winthrop, K., and Gottlieb, R.L. (2021). Neutralizing monoclonal antibodies for treatment of COVID-19. Nat. Rev. Immunol. *21*, 382–393. https://doi.org/10.1038/s41577-021-00542-x.
5. Pantaleo, G., Correia, B., Fenwick, C., Joo, V.S., and Perez, L. (2022). Antibodies to combat viral infections: development strategies and progress. Nat. Rev. Drug Discov. *21*, 676–696. https://doi.org/10.1038/s41573-022-00495-3.
6. Chen, Y., Zhao, X., Zhou, H., Zhu, H., Jiang, S., and Wang, P. (2023). Broadly neutralizing antibodies to SARS-CoV-2 and other human coronaviruses. Nat. Rev. Immunol. *23*, 189–199. https://doi.org/10.1038/s41577-022-00784-3.
7. Cao, Y., Su, B., Guo, X., Sun, W., Deng, Y., Bao, L., Zhu, Q., Zhang, X., Zheng, Y., Geng, C., et al. (2020). Potent Neutralizing Antibodies against SARS-CoV-2 Identified by High-Throughput Single-Cell Sequencing of Convalescent Patients' B Cells. Cell *182*, 73–84.e16. https://doi.org/10.1016/j.cell.2020.05.025.
8. Zost, S.J., Gilchuk, P., Case, J.B., Binshtein, E., Chen, R.E., Nkolola, J.P., Schäfer, A., Reidy, J.X., Trivette, A., Nargi, R.S., et al. (2020). Potently neutralizing and protective human antibodies against SARS-CoV-2. Nature *584*, 443–449. https://doi.org/10.1038/s41586-020-2548-6.
9. Wec, A.Z., Wrapp, D., Herbert, A.S., Maurer, D.P., Haslwanter, D., Sakharkar, M., Jangra, R.K., Dieterle, M.E., Lilov, A., Huang, D., et al. (2020). Broad neutralization of SARS-related viruses by human monoclonal antibodies. Science *369*, 731–736. https://doi.org/10.1126/science.abc7424.
10. Pinto, D., Park, Y.-J., Beltramello, M., Walls, A.C., Tortorici, M.A., Bianchi, S., Jaconi, S., Culap, K., Zatta, F., De Marco, A., et al. (2020). Cross-neutralization of SARS-CoV-2 by a human monoclonal SARS-CoV antibody. Nature *583*, 290–295. https://doi.org/10.1038/s41586-020-2349-y.
11. He, W.T., Musharrafieh, R., Song, G., Dueker, K., Tse, L.V., Martinez, D.R., Schäfer, A., Callaghan, S., Yong, P., Beutler, N., et al. (2022). Targeted isolation of diverse human protective broadly neutralizing antibodies against SARS-like viruses. Nat. Immunol. *23*, 960–970. https://doi.org/10.1038/s41590-022-01222-1.
12. Haslwanter, D., Dieterle, M.E., Wec, A.Z., O'Brien, C.M., Sakharkar, M., Florez, C., Tong, K., Rappazzo, C.G., Lasso, G., Vergnolle, O., et al. (2021). A Combination of Receptor-Binding Domain and N-Terminal Domain Neutralizing Antibodies Limits the Generation of SARS-CoV-2 Spike Neutralization-Escape Mutants. mBio *12*, e0247321. https://doi.org/10.1128/mBio.02473-21.
13. McCallum, M., De Marco, A., Lempp, F.A., Tortorici, M.A., Pinto, D., Walls, A.C., Beltramello, M., Chen, A., Liu, Z., Zatta, F., et al. (2021). N-terminal domain antigenic mapping reveals a site of vulnerability for SARS-CoV-2. Cell *184*, 2332–2347.e16. https://doi.org/10.1016/j.cell.2021.03.028.
14. Liu, Y., Soh, W.T., Kishikawa, J.I., Hirose, M., Nakayama, E.E., Li, S., Sasai, M., Suzuki, T., Tada, A., Arakawa, A., et al. (2021). An infectivity-enhancing site on the SARS-CoV-2 spike protein targeted by antibodies. Cell *184*, 3452–3466.e18. https://doi.org/10.1016/j.cell.2021.05.032.
15. Jennewein, M.F., MacCamy, A.J., Akins, N.R., Feng, J., Homad, L.J., Hurlburt, N.K., Seydoux, E., Wan, Y.-H., Stuart, A.B., Edara, V.V., et al. (2021). Isolation and characterization of cross-neutralizing coronavirus antibodies from COVID-19+ subjects. Cell Rep. *36*, 109353. https://doi.org/10.1016/j.celrep.2021.109353.
16. Graham, C., Seow, J., Huettner, I., Khan, H., Kouphou, N., Acors, S., Winstone, H., Pickering, S., Galao, R.P., Dupont, L., et al. (2021). Neutralization potency of monoclonal antibodies recognizing dominant and subdominant epitopes on SARS-CoV-2 Spike is impacted by the B.1.1.7 variant. Immunity *54*, 1276–1289.e6. https://doi.org/10.1016/j.immuni.2021.03.023.
17. Wang, Z., Schmidt, F., Weisblum, Y., Muecksch, F., Barnes, C.O., Finkin, S., Schaefer-Babajew, D., Cipolla, M., Gaebler, C., Lieberman, J.A., et al. (2021). mRNA vaccine-elicited antibodies to SARS-CoV-2 and circulating variants. Nature *592*, 616–622. https://doi.org/10.1038/s41586-021-03324-6.
18. Collier, D.A., De Marco, A., Ferreira, I.A.T.M., Meng, B., Datir, R.P., Walls, A.C., Kemp, S.A., Bassi, J., Pinto, D., Silacci-Fregni, C., et al. (2021). Sensitivity of SARS-CoV-2 B.1.1.7 to mRNA vaccine-elicited antibodies. Nature *593*, 136–141. https://doi.org/10.1038/s41586-021-03412-7.
19. Wang, P., Nair, M.S., Liu, L., Iketani, S., Luo, Y., Guo, Y., Wang, M., Yu, J., Zhang, B., Kwong, P.D., et al. (2021). Antibody resistance of SARS-CoV-2 variants B.1.351 and B.1.1.7. Nature *593*, 130–135. https://doi.org/10.1038/s41586-021-03398-2.
20. Kaku, Y., Kuwata, T., Zahid, H.M., Hashiguchi, T., Noda, T., Kuramoto, N., Biswas, S., Matsumoto, K., Shimizu, M., Kawanami, Y., et al. (2021). Resistance of SARS-CoV-2 variants to neutralization by antibodies induced in convalescent patients with COVID-19. Cell Rep. *36*, 109385. https://doi.org/10.1016/j.celrep.2021.109385.
21. Kurhade, C., Zou, J., Xia, H., Liu, M., Chang, H.C., Ren, P., Xie, X., and Shi, P.Y. (2023). Low neutralization of SARS-CoV-2 Omicron BA.2.75.2, BQ.1.1 and XBB.1 by parental mRNA vaccine or a BA.5 bivalent booster. Nat. Med. *29*, 344–347. https://doi.org/10.1038/s41591-022-02162-x.
22. Akerman, A., Milogiannakis, V., Jean, T., Esneau, C., Silva, M.R., Ison, T., Fichter, C., Lopez, J.A., Chandra, D., Naing, Z., et al. (2023). Emergence and antibody evasion of BQ, BA.2.75 and SARS-CoV-2 recombinant sub-lineages in the face of maturing antibody breadth at the population level. EBioMedicine *90*, 104545. https://doi.org/10.1016/j.ebiom.2023.104545.
23. Planas, D., Saunders, N., Maes, P., Guivel-Benhassine, F., Planchais, C., Buchrieser, J., Bolland, W.-H., Porrot, F., Staropoli, I., Lemoine, F., et al. (2022). Considerable escape of SARS-CoV-2 Omicron to antibody neutralization. Nature *602*, 671–675. https://doi.org/10.1038/s41586-021-04389-z.
24. Wang, Q., Guo, Y., Iketani, S., Nair, M.S., Li, Z., Mohri, H., Wang, M., Yu, J., Bowen, A.D.,

Chang, J.Y., et al. (2022). Antibody evasion by SARS-CoV-2 Omicron subvariants BA.2.12.1, BA.4 and BA.5. Nature *608*, 603–608. https://doi.org/10.1038/s41586-022-05053-w.

25. Gruell, H., Vanshylla, K., Korenkov, M., Tober-Lau, P., Zehner, M., Münn, F., Janicki, H., Augustin, M., Schommers, P., Sander, L.E., et al. (2022). SARS-CoV-2 Omicron sublineages exhibit distinct antibody escape patterns. Cell Host Microbe *30*, 1231–1241.e6. https://doi.org/10.1016/j.chom.2022.07.002.
26. Planas, D., Bruel, T., Staropoli, I., Guivel-Benhassine, F., Porrot, F., Maes, P., Grzelak, L., Prot, M., Mougari, S., Planchais, C., et al. (2023). Resistance of Omicron subvariants BA.2.75.2, BA.4.6, and BQ.1.1 to neutralizing antibodies. Nat. Commun. *14*, 824. https://doi.org/10.1038/s41467-023-36561-6.
27. Guo, H., Jiang, J., Shen, S., Ge, X., Fan, Q., Zhou, B., Cheng, L., Ju, B., and Zhang, Z. (2023). Additional mutations based on Omicron BA.2.75 mediate its further evasion from broadly neutralizing antibodies. iScience *26*, 106283. https://doi.org/10.1016/j.isci.2023.106283.
28. Wang, Q., Iketani, S., Li, Z., Guo, Y., Yeh, A.Y., Liu, M., Yu, J., Sheng, Z., Huang, Y., Liu, L., and Ho, D.D. (2022). Antigenic characterization of the SARS-CoV-2 Omicron subvariant BA.2.75. Cell Host Microbe *30*, 1512–1517.e4. https://doi.org/10.1016/j.chom.2022.09.002.
29. Westendorf, K., Žentelis, S., Wang, L., Foster, D., Vaillancourt, P., Wiggin, M., Lovett, E., van der Lee, R., Hendle, J., Pustilnik, A., et al. (2022). LY-CoV1404 (bebtelovimab) potently neutralizes SARS-CoV-2 variants. Cell Rep. *39*, 110812. https://doi.org/10.1016/j.celrep.2022.110812.
30. Wang, Q., Iketani, S., Li, Z., Liu, L., Guo, Y., Huang, Y., Bowen, A.D., Liu, M., Wang, M., Yu, J., et al. (2023). Alarming antibody evasion properties of rising SARS-CoV-2 BQ and XBB subvariants. Cell *186*, 279–286.e8. https://doi.org/10.1016/j.cell.2022.12.018.
31. Touret, F., Giraud, E., Bourret, J., Donati, F., Tran-Rajau, J., Chiaravalli, J., Lemoine, F., Agou, F., Simon-Lorière, E., van der Werf, S., and de Lamballerie, X. (2023). Enhanced neutralization escape to therapeutic monoclonal antibodies by SARS-CoV-2 omicron sub-lineages. iScience *26*, 106413. https://doi.org/10.1016/j.isci.2023.106413.
32. Logtenberg, T. (2007). Antibody cocktails: next-generation biopharmaceuticals with improved potency. Trends Biotechnol. *25*, 390–394. https://doi.org/10.1016/j.tibtech.2007.07.005.
33. Baum, A., Fulton, B.O., Wloga, E., Copin, R., Pascal, K.E., Russo, V., Giordano, S., Lanza, K., Negron, N., Ni, M., et al. (2020). Antibody cocktail to SARS-CoV-2 spike protein prevents rapid mutational escape seen with individual antibodies. Science *369*, 1014–1018. https://doi.org/10.1126/science.abd0831.
34. Pinto, D., Sauer, M.M., Czudnochowski, N., Low, J.S., Tortorici, M.A., Housley, M.P., Noack, J., Walls, A.C., Bowen, J.E., Guarino, B., et al. (2021). Broad betacoronavirus neutralization by a stem helix–specific human antibody. Science *373*, 1109–1116. https://doi.org/10.1126/science.abj3321.
35. Sauer, M.M., Tortorici, M.A., Park, Y.-J., Walls, A.C., Homad, L., Acton, O.J., Bowen, J.E., Wang, C., Xiong, X., de van der Schueren, W., et al. (2021). Structural basis for broad coronavirus neutralization. Nat. Struct. Mol. Biol. *28*, 478–486. https://doi.org/10.1038/s41594-021-00596-4.
36. Zhou, P., Yuan, M., Song, G., Beutler, N., Shaabani, N., Huang, D., He, W.T., Zhu, X., Callaghan, S., Yong, P., et al. (2022). A human antibody reveals a conserved site on beta-coronavirus spike proteins and confers protection against SARS-CoV-2 infection. Sci. Transl. Med. *14*, eabi9215. https://doi.org/10.1126/scitranslmed.abi9215.
37. Piepenbrink, M.S., Park, J.-G., Deshpande, A., Loos, A., Ye, C., Basu, M., Sarkar, S., Khalil, A.M., Chauvin, D., Woo, J., et al. (2022). Potent universal beta-coronavirus therapeutic activity mediated by direct respiratory administration of a Spike S2 domain-specific human neutralizing monoclonal antibody. PLoS Pathog. *18*, e1010691. https://doi.org/10.1371/journal.ppat.1010691.
38. Li, C.-J., Chao, T.-L., Chang, T.-Y., Hsiao, C.-C., Lu, D.-C., Chiang, Y.-W., Lai, G.-C., Tsai, Y.-M., Fang, J.-T., Ieong, S., et al. (2022). Neutralizing Monoclonal Antibodies Inhibit SARS-CoV-2 Infection through Blocking Membrane Fusion. Microbiol. Spectr. *10*, e0181421. https://doi.org/10.1128/spectrum.01814-21.
39. Li, W., Chen, Y., Prévost, J., Ullah, I., Lu, M., Gong, S.Y., Tauzin, A., Gasser, R., Vézina, D., Anand, S.P., et al. (2022). Structural basis and mode of action for two broadly neutralizing antibodies against SARS-CoV-2 emerging variants of concern. Cell Rep. *38*, 110210. https://doi.org/10.1016/j.celrep.2021.110210.
40. Zhou, P., Song, G., Liu, H., Yuan, M., He, W.T., Beutler, N., Zhu, X., Tse, L.V., Martinez, D.R., Schäfer, A., et al. (2023). Broadly neutralizing anti-S2 antibodies protect against all three human betacoronaviruses that cause deadly disease. Immunity *56*, 669–686.e7. https://doi.org/10.1016/j.immuni.2023.02.005.
41. Wu, W.-L., Chiang, C.-Y., Lai, S.-C., Yu, C.-Y., Huang, Y.-L., Liao, H.-C., Liao, C.-L., Chen, H.-W., and Liu, S.-J. (2022). Monoclonal antibody targeting the conserved region of the SARS-CoV-2 spike protein to overcome viral variants. JCI Insight *7*, e157597. https://doi.org/10.1172/jci.insight.157597.
42. Weidenbacher, P.A.-B., Waltari, E., de los Rios Kobara, I., Bell, B.N., Morris, M.K., Cheng, Y.-C., Hanson, C., Pak, J.E., and Kim, P.S. (2022). Converting non-neutralizing SARS-CoV-2 antibodies into broad-spectrum inhibitors. Nat. Chem. Biol. *18*, 1270–1276. https://doi.org/10.1038/s41589-022-01140-1.
43. Lim, S.A., Gramespacher, J.A., Pance, K., Rettko, N.J., Solomon, P., Jin, J., Lui, I., Elledge, S.K., Liu, J., Bracken, C.J., et al. (2021). Bispecific VH/Fab antibodies targeting neutralizing and non-neutralizing Spike epitopes demonstrate enhanced potency against SARS-CoV-2. mAbs *13*, 1893426. https://doi.org/10.1080/19420862.2021.1893426.
44. Yuan, M., Chen, X., Zhu, Y., Dong, X., Liu, Y., Qian, Z., Ye, L., and Liu, P. (2022). A Bispecific Antibody Targeting RBD and S2 Potently Neutralizes SARS-CoV-2 Omicron and Other Variants of Concern. J. Virol. *96*, e0077522. https://doi.org/10.1128/jvi.00775-22.
45. Meng, B., Abdullahi, A., Ferreira, I.A.T.M., Goonawardane, N., Saito, A., Kimura, I., Yamasoba, D., Gerber, P.P., Fatihi, S., Rathore, S., et al. (2022). Altered TMPRSS2 usage by SARS-CoV-2 Omicron impacts infectivity and fusogenicity. Nature *603*, 706–714. https://doi.org/10.1038/s41586-022-04474-x.
46. Suzuki, R., Yamasoba, D., Kimura, I., Wang, L., Kishimoto, M., Ito, J., Morioka, Y., Nao, N., Nasser, H., Uriu, K., et al. (2022). Attenuated fusogenicity and pathogenicity of SARS-CoV-2 Omicron variant. Nature *603*, 700–705. https://doi.org/10.1038/s41586-022-04462-1.
47. Li, C.-J., and Chang, S.-C. (2023). SARS-CoV-2 spike S2-specific neutralizing antibodies. Emerg. Microb. Infect. *12*, 2220582. https://doi.org/10.1080/22221751.2023.2220582.
48. Jackson, C.B., Farzan, M., Chen, B., and Choe, H. (2022). Mechanisms of SARS-CoV-2 entry into cells. Nat. Rev. Mol. Cell Biol. *23*, 3–20. https://doi.org/10.1038/s41580-021-00418-x.
49. Willett, B.J., Grove, J., MacLean, O.A., Wilkie, C., De Lorenzo, G., Furnon, W., Cantoni, D., Scott, S., Logan, N., Ashraf, S., et al. (2022). SARS-CoV-2 Omicron is an immune escape variant with an altered cell entry pathway. Nat. Microbiol. *7*, 1161–1179. https://doi.org/10.1038/s41564-022-01143-7.
50. Neerukonda, S.N., Wang, R., Vassell, R., Baha, H., Lusvarghi, S., Liu, S., Wang, T., Weiss, C.D., and Wang, W. (2022). Characterization of Entry Pathways, Species-Specific Angiotensin-Converting Enzyme 2 Residues Determining Entry, and Antibody Neutralization Evasion of Omicron BA.1, BA.1.1, BA.2, and BA.3 Variants. J. Virol. *96*, e0114022. https://doi.org/10.1128/jvi.01140-22.
51. Iwata-Yoshikawa, N., Kakizaki, M., Shiwa-Sudo, N., Okura, T., Tahara, M., Fukushi, S., Maeda, K., Kawase, M., Asanuma, H., Tomita, Y., et al. (2022). Essential role of TMPRSS2 in SARS-CoV-2 infection in murine airways. Nat. Commun. *13*, 6100. https://doi.org/10.1038/s41467-022-33911-8.
52. Matsuyama, S., Nao, N., Shirato, K., Kawase, M., Saito, S., Takayama, I., Nagata, N., Sekizuka, T., Katoh, H., Kato, F., et al. (2020). Enhanced isolation of SARS-CoV-2 by TMPRSS2-expressing cells. Proc. Natl. Acad. Sci. USA *117*, 7001–7003. https://doi.org/10.1073/pnas.2002589117.
53. Kodaka, M., Yang, Z., Nakagawa, K., Maruyama, J., Xu, X., Sarkar, A., Ichimura, A., Nasu, Y., Ozawa, T., Iwasa, H., et al. (2015). A new cell-based assay to evaluate myogenesis in mouse myoblast C2C12 cells. Exp. Cell Res. *336*, 171–181. https://doi.org/10.1016/j.yexcr.2015.06.015.
54. Feng, S., Sekine, S., Pessino, V., Li, H., Leonetti, M.D., and Huang, B. (2017). Improved split fluorescent proteins for endogenous protein labeling. Nat. Commun. *8*, 370. https://doi.org/10.1038/s41467-017-00494-8.
55. Takashita, E., Yamayoshi, S., Simon, V., van Bakel, H., Sordillo, E.M., Pekosz, A., Fukushi, S., Suzuki, T., Maeda, K., Halfmann, P., et al. (2022). Efficacy of Antibodies and Antiviral Drugs against Omicron BA.2.12.1, BA.4, and BA.5 Subvariants. N. Engl. J. Med. *387*, 468–470. https://doi.org/10.1056/NEJMc2207519.
56. Cox, M., Peacock, T.P., Harvey, W.T., Hughes, J., Wright, D.W., COVID-19 Genomics UK COG-UK Consortium, Willett, B.J., Thomson, E., Gupta, R.K., Peacock, S.J., et al. (2023). SARS-CoV-2 variant evasion of monoclonal antibodies based on in vitro studies. Nat. Rev. Microbiol. *21*, 112–124. https://doi.org/10.1038/s41579-022-00809-7.
57. Ambrose, N., Amin, A., Anderson, B., Barrera-Oro, J., Bertagnolli, M., Campion, F., Chow,

D., Danan, R., D'Arinzo, L., Drews, A., et al. (2023). Neutralizing Monoclonal Antibody Use and COVID-19 Infection Outcomes. JAMA Netw. Open *6*, e239694. https://doi.org/10.1001/jamanetworkopen.2023.9694.

58. Ai, J., Wang, X., He, X., Zhao, X., Zhang, Y., Jiang, Y., Li, M., Cui, Y., Chen, Y., Qiao, R., et al. (2022). Antibody evasion of SARS-CoV-2 Omicron BA.1, BA.1.1, BA.2, and BA.3 sub-lineages. Cell Host Microbe *30*, 1077–1083.e4. https://doi.org/10.1016/j.chom.2022.05.001.
59. Takeshita, M., Fukuyama, H., Kamada, K., Matsumoto, T., Makino-Okamura, C., Uchikubo-Kamo, T., Tomabechi, Y., Hanada, K., Moriyama, S., Takahashi, Y., et al. (2022). Potent SARS-CoV-2 neutralizing antibodies with therapeutic effects in two animal models. iScience *25*, 105596. https://doi.org/10.1016/j.isci.2022.105596.
60. Onodera, T., Kita, S., Adachi, Y., Moriyama, S., Sato, A., Nomura, T., Sakakibara, S., Inoue, T., Tadokoro, T., Anraku, Y., et al. (2021). A SARS-CoV-2 antibody broadly neutralizes SARS-related coronaviruses and variants by coordinated recognition of a virus-vulnerable site. Immunity *54*, 2385–2398.e10. https://doi.org/10.1016/j.immuni.2021.08.025.
61. Jensen, J.L., Sankhala, R.S., Dussupt, V., Bai, H., Hajduczki, A., Lal, K.G., Chang, W.C., Martinez, E.J., Peterson, C.E., Golub, E.S., et al. (2023). Targeting the Spike Receptor Binding Domain Class V Cryptic Epitope by an Antibody with Pan-Sarbecovirus Activity. J. Virol. *97*, e0159622. https://doi.org/10.1128/jvi.01596-22.
62. Ishimaru, H., Nishimura, M., Tjan, L.H., Sutandhio, S., Marini, M.I., Effendi, G.B., Shigematsu, H., Kato, K., Hasegawa, N., Aoki, K., et al. (2023). Identification and Analysis of Monoclonal Antibodies with Neutralizing Activity against Diverse SARS-CoV-2 Variants. J. Virol. *97*, e0028623. https://doi.org/10.1128/jvi.00286-23.
63. Ju, B., Zhang, Q., Wang, Z., Aw, Z.Q., Chen, P., Zhou, B., Wang, R., Ge, X., Lv, Q., Cheng, L., et al. (2023). Infection with wild-type SARS-CoV-2 elicits broadly neutralizing and protective antibodies against omicron subvariants. Nat. Immunol. *24*, 690–699. https://doi.org/10.1038/s41590-023-01449-6.
64. Huang, K.-Y.A., Chen, X., Mohapatra, A., Nguyen, H.T.V., Schimanski, L., Tan, T.K., Rijal, P., Vester, S.K., Hills, R.A., Howarth, M., et al. (2023). Structural basis for a conserved neutralization epitope on the receptor-binding domain of SARS-CoV-2. Nat. Commun. *14*, 311. https://doi.org/10.1038/s41467-023-35949-8.
65. Cameroni, E., Bowen, J.E., Rosen, L.E., Saliba, C., Zepeda, S.K., Culap, K., Pinto, D., VanBlargan, L.A., De Marco, A., di Iulio, J., et al. (2022). Broadly neutralizing antibodies overcome SARS-CoV-2 Omicron antigenic shift. Nature *602*, 664–670. https://doi.org/10.1038/s41586-021-04386-2.
66. Moriyama, S., Anraku, Y., Taminishi, S., Adachi, Y., Kuroda, D., Kita, S., Higuchi, Y., Kirita, Y., Kotaki, R., Tonouchi, K., et al. (2023). Structural delineation and computational design of SARS-CoV-2-neutralizing antibodies against Omicron subvariants. Nat. Commun. *14*, 4198. https://doi.org/10.1038/s41467-023-39890-8.
67. Wang, Y., Zhang, X., Ma, Y., Wang, Y., Zhan, W., Zheng, Q., Zhang, M., Ji, P., Liu, M., Liu, Q., et al. (2022). Combating the SARS-CoV-2 Omicron (BA.1) and BA.2 with potent bispecific antibodies engineered from non-Omicron neutralizing antibodies. Cell Discov. *8*, 104. https://doi.org/10.1038/s41421-022-00463-6.
68. Chang, M.R., Tomasovic, L., Kuzmina, N.A., Ronk, A.J., Byrne, P.O., Johnson, R., Storm, N., Olmedillas, E., Hou, Y.J., Schäfer, A., et al. (2022). IgG-like bispecific antibodies with potent and synergistic neutralization against circulating SARS-CoV-2 variants of concern. Nat. Commun. *13*, 5814. https://doi.org/10.1038/s41467-022-33030-4.
69. Ku, Z., Xie, X., Lin, J., Gao, P., Wu, B., El Sahili, A., Su, H., Liu, Y., Ye, X., Tan, E.Y., et al. (2022). Engineering SARS-CoV-2 specific cocktail antibodies into a bispecific format improves neutralizing potency and breadth. Nat. Commun. *13*, 5552. https://doi.org/10.1038/s41467-022-33284-y.
70. Kim, J.W., Heo, K., Kim, H.J., Yoo, Y., Cho, H.-S., Jang, H.J., Lee, H.-Y., Ko, I.Y., Woo, J.R., Cho, Y.B., et al. (2023). Novel bispecific human antibody platform specifically targeting a fully open spike conformation potently neutralizes multiple SARS-CoV-2 variants. Antivir. Res. *212*, 105576. https://doi.org/10.1016/j.antiviral.2023.105576.
71. Radić, L., Sliepen, K., Yin, V., Brinkkemper, M., Capella-Pujol, J., Schriek, A.I., Torres, J.L., Bangaru, S., Burger, J.A., Poniman, M., et al. (2023). Bispecific antibodies combine breadth, potency, and avidity of parental antibodies to neutralize sarbecoviruses. iScience *26*, 106540. https://doi.org/10.1016/j.isci.2023.106540.
72. Li, Z., Li, S., Zhang, G., Peng, W., Chang, Z., Zhang, X., Fan, Z., Chai, Y., Wang, F., Zhao, X., et al. (2022). An engineered bispecific human monoclonal antibody against SARS-CoV-2. Nat. Immunol. *23*, 423–430. https://doi.org/10.1038/s41590-022-01138-w.
73. Cho, H., Gonzales-Wartz, K.K., Huang, D., Yuan, M., Peterson, M., Liang, J., Beutler, N., Torres, J.L., Cong, Y., Postnikova, E., et al. (2021). Bispecific antibodies targeting distinct regions of the spike protein potently neutralize SARS-CoV-2 variants of concern. Sci. Transl. Med. *13*, eabj5413. https://doi.org/10.1126/scitranslmed.abj5413.
74. De Gasparo, R., Pedotti, M., Simonelli, L., Nickl, P., Muecksch, F., Cassaniti, I., Percivalle, E., Lorenzi, J.C.C., Mazzola, F., Magrì, D., et al. (2021). Bispecific IgG neutralizes SARS-CoV-2 variants and prevents escape in mice. Nature *593*, 424–428. https://doi.org/10.1038/s41586-021-03461-y.
75. Zhang, J., Xiao, T., Cai, Y., and Chen, B. (2021). Structure of SARS-CoV-2 spike protein. Curr. Opin. Virol. *50*, 173–182. https://doi.org/10.1016/j.coviro.2021.08.010.
76. Cai, Y., Zhang, J., Xiao, T., Peng, H., Sterling, S.M., Walsh, R.M., Rawson, S., Rits-Volloch, S., and Chen, B. (2020). Distinct conformational states of SARS-CoV-2 spike protein. Science *369*, 1586–1592. https://doi.org/10.1126/science.abd4251.
77. Yuan, Y., Cao, D., Zhang, Y., Ma, J., Qi, J., Wang, Q., Lu, G., Wu, Y., Yan, J., Shi, Y., et al. (2017). Cryo-EM structures of MERS-CoV and SARS-CoV spike glycoproteins reveal the dynamic receptor binding domains. Nat. Commun. *8*, 15092. https://doi.org/10.1038/ncomms15092.
78. Fan, X., Cao, D., Kong, L., and Zhang, X. (2020). Cryo-EM analysis of the post-fusion structure of the SARS-CoV spike glycoprotein. Nat. Commun. *11*, 3618. https://doi.org/10.1038/s41467-020-17371-6.
79. Marcink, T.C., Kicmal, T., Armbruster, E., Zhang, Z., Zipursky, G., Golub, K.L., Idris, M., Khao, J., Drew-Bear, J., McGill, G., et al. (2022). Intermediates in SARS-CoV-2 spike–mediated cell entry. Sci. Adv. *8*, eabo3153. https://doi.org/10.1126/sciadv.abo3153.
80. Hurlburt, N.K., Homad, L.J., Sinha, I., Jennewein, M.F., MacCamy, A.J., Wan, Y.-H., Boonyaratanakornkit, J., Sholukh, A.M., Jackson, A.M., Zhou, P., et al. (2022). Structural definition of a pan-sarbecovirus neutralizing epitope on the spike S2 subunit. Commun. Biol. *5*, 342. https://doi.org/10.1038/s42003-022-03262-7.
81. Seifert, S.N., Bai, S., Fawcett, S., Norton, E.B., Zwezdaryk, K.J., Robinson, J., Gunn, B., and Letko, M. (2022). An ACE2-dependent Sarbecovirus in Russian bats is resistant to SARS-CoV-2 vaccines. PLoS Pathog. *18*, e1010828. https://doi.org/10.1371/journal.ppat.1010828.
82. Luo, S., Zhang, J., Kreutzberger, A.J.B., Eaton, A., Edwards, R.J., Jing, C., Dai, H.-Q., Sempowski, G.D., Cronin, K., Parks, R., et al. (2022). An antibody from single human V_H-rearranging mouse neutralizes all SARS-CoV-2 variants through BA.5 by inhibiting membrane fusion. Sci. Immunol. *7*, eadd5446. https://doi.org/10.1126/sciimmunol.add5446.
83. Huo, J., Dijokaite-Guraliuc, A., Liu, C., Zhou, D., Ginn, H.M., Das, R., Supasa, P., Selvaraj, M., Nutalai, R., Tuekprakhon, A., et al. (2023). A delicate balance between antibody evasion and ACE2 affinity for Omicron BA.2.75. Cell Rep. *42*, 111903. https://doi.org/10.1016/j.celrep.2022.111903.
84. Saito, A., Tamura, T., Zahradnik, J., Deguchi, S., Tabata, K., Anraku, Y., Kimura, I., Ito, J., Yamasoba, D., Nasser, H., et al. (2022). Virological characteristics of the SARS-CoV-2 Omicron BA.2.75 variant. Cell Host Microbe *30*, 1540–1555.e15. https://doi.org/10.1016/j.chom.2022.10.003.
85. Zhang, Y.-Y., Liang, R., Wang, S.-J., Ye, Z.-W., Wang, T.-Y., Chen, M., Liu, J., Na, L., Yang, Y.-L., Yang, Y.-B., et al. (2022). SARS-CoV-2 hijacks macropinocytosis to facilitate its entry and promote viral spike–mediated cell-to-cell fusion. J. Biol. Chem. *298*, 102511. https://doi.org/10.1016/j.jbc.2022.102511.
86. Bayati, A., Kumar, R., Francis, V., and herson, P.S. (2021). SARS-CoV-2 infects cells after viral entry via clathrin-mediated endocytosis. J. Biol. Chem. *296*, 100306. https://doi.org/10.1016/j.jbc.2021.100306.
87. Winkler, E.S., Gilchuk, P., Yu, J., Bailey, A.L., Chen, R.E., Chong, Z., Zost, S.J., Jang, H., Huang, Y., Allen, J.D., et al. (2021). Human neutralizing antibodies against SARS-CoV-2 require intact Fc effector functions for optimal therapeutic protection. Cell *184*, 1804–1820.e16. https://doi.org/10.1016/j.cell.2021.02.026.
88. Zhang, A., Stacey, H.D., D'Agostino, M.R., Tugg, Y., Marzok, A., and Miller, M.S. (2023). Beyond neutralization: Fc-dependent antibody effector functions in SARS-CoV-2 infection. Nat. Rev. Immunol. *23*, 381–396. https://doi.org/10.1038/s41577-022-00813-1.
89. Grant, M.D., Bentley, K., Fielding, C.A., Hatfield, K.M., Ings, D.P., Harnum, D., Wang, E.C., Stanton, R.J., and Holder, K.A. (2023). Combined anti-S1 and anti-S2 antibodies from hybrid immunity elicit potent cross-variant ADCC against SARS-CoV-2. JCI Insight *8*, e170681. https://doi.org/10.1172/jci.insight.170681.

90. Coloma, M.J., and Morrison, S.L. (1997). Design and production of novel tetravalent bispecific antibodies. Nat. Biotechnol. *15*, 159–163. https://doi.org/10.1038/nbt0297-159.

91. Frentzas, S., Gan, H.K., Cosman, R., Coward, J., Tran, B., Millward, M., Zhou, Y., Wang, W., Xia, D., Wang, Z.M., et al. (2023). A phase 1a/1b first-in-human study (COMPASSION-01) evaluating cadonilimab in patients with advanced solid tumors. Cell Rep. Med. *4*, 101242. https://doi.org/10.1016/j.xcrm.2023.101242.

92. Yamamoto, Y., Inoue, T., Inoue, M., Murae, M., Fukasawa, M., Kaneko, M.K., Kato, Y., and Noguchi, K. (2022). SARS-CoV-2 Spike Protein Mutation at Cysteine-488 Impairs Its Golgi Localization and Intracellular S1/S2 Processing. Int. J. Mol. Sci. *23*, 15834. https://doi.org/10.3390/ijms232415834.

93. Murae, M., Shimizu, Y., Yamamoto, Y., Kobayashi, A., Houri, M., Inoue, T., Irie, T., Gemba, R., Kondo, Y., Nakano, Y., et al. (2022). The function of SARS-CoV-2 spike protein is impaired by disulfide-bond disruption with mutation at cysteine-488 and by thiol-reactive N-acetyl-cysteine and glutathione. Biochem. Biophys. Res. Commun. *597*, 30–36. https://doi.org/10.1016/j.bbrc.2022.01.106.

94. Rafique, S., Idrees, M., Ali, A., Sahibzada, K.I., and Iqbal, M. (2014). Generation of infectious HCV pseudo typed particles and its utilization for studying the role of CD81 & SRBI receptors in HCV infection. Mol. Biol. Rep. *41*, 3813–3819. https://doi.org/10.1007/s11033-014-3247-x.

95. Pettersen, E.F., Goddard, T.D., Huang, C.C., Couch, G.S., Greenblatt, D.M., Meng, E.C., and Ferrin, T.E. (2004). UCSF Chimera—A visualization system for exploratory research and analysis. J. Comput. Chem. *25*, 1605–1612. https://doi.org/10.1002/jcc.20084.

96. Waterhouse, A.M., Procter, J.B., Martin, D.M.A., Clamp, M., and Barton, G.J. (2009). Jalview Version 2—a multiple sequence alignment editor and analysis workbench. Bioinformatics *25*, 1189–1191. https://doi.org/10.1093/bioinformatics/btp033.

97. Dufloo, J., Grzelak, L., Staropoli, I., Madec, Y., Tondeur, L., Anna, F., Pelleau, S., Wiedemann, A., Planchais, C., Buchrieser, J., et al. (2021). Asymptomatic and symptomatic SARS-CoV-2 infections elicit polyfunctional antibodies. Cell Rep. Med. *2*, 100275. https://doi.org/10.1016/j.xcrm.2021.100275.

98. Bruel, T., Stéfic, K., Nguyen, Y., Toniutti, D., Staropoli, I., Porrot, F., Guivel-Benhassine, F., Bolland, W.-H., Planas, D., Hadjadj, J., et al. (2022). Longitudinal analysis of serum neutralization of SARS-CoV-2 Omicron BA.2, BA.4, and BA.5 in patients receiving monoclonal antibodies. Cell Rep. Med. *3*, 100850. https://doi.org/10.1016/j.xcrm.2022.100850.

STAR★METHODS

KEY RESOURCES TABLE

REAGENT or RESOURCE	SOURCE	IDENTIFIER
Antibodies		
CvMab-6	Yamamoto et al.[92]	N/A
CvMab-62	This study	N/A
Humanized CvMab-62	This study	N/A
Bebtelovimab (LY-CoV1404)	Westendorf et al.[29]	N/A
Bis1	This study	N/A
Bis2	This study	N/A
Bis3	This study	N/A
Bis4	This study	N/A
Bis-Bebtelovimab (Bis-beb)	This study	N/A
Humanized Bis-Beb	This study	N/A
SARS-CoV-2 anti-spike (clone 1A9)	GeneTex Inc.	Cat# GTX632604
Anti-coronavirus spike S2 antibody	Sino Biological Inc.	Cat# 40590-T62
Cleaved SARS-CoV-2 S (Ser 686) Antibody	Cell Signaling Technology	Cat# 84534
Anti-GAPDH (clone 3H12)	Medical & Biological Laboratories Co., Ltd	Cat# 171-3
Horse anti-mouse IgG-HRP	Cell Signaling Technology	Cat# 7076
Goat anti-mouse IgG-HRP	Proteintech Group	Cat# SA00001-1
Anti-rabbit IgG-HRP	Cytiva™	Cat# NA934
Anti-His-tag mAb-HRP-DirecT	MBL	Cat# D291-7
Goat anti-mouse IgG (H + L) cross-adsorbed with Alexa Fluor® 488	Thermo Fisher Scientific	Cat# A-11001
Anti-CD20 antibody	Promega corp.	Cat# GA1130
Bacterial and virus strains		
SARS-CoV-2 wuhan	2019-nCoV/Japan/TY/WK-521/2020	GISAID ID# EPI_ISL_408667
SARS-CoV-2 Alpha B.1.1.7	hCoV-19/Japan/QHN001/2020	GISAID ID# EPI_ISL_804007
SARS-CoV-2 Delta B.1.617.2	hCoV-19/Japan/TY11-927/2021	GISAID ID# EPI_ISL_2158617
SARS-CoV-2 Omicron BA.1	hCoV-19/Japan/TY38-873/2021	GISAID ID# EPI_ISL_7418017
SARS-CoV-2 Omicron BA.5.2.1	hCoV-19/Japan/TY41-704/2022	GISAID ID# EPI_ISL_13241868
SARS-CoV-2 BQ.1	hCoV-19/Japan/TY41-796/2022	GISAID ID# EPI_ISL_15579783
Chemicals, peptides, and recombinant proteins		
Trimeric SARS-CoV-2 Spike Wuhan	Sino Biological Inc.	Cat# 40589-V08H4
Trimeric SARS-CoV-2 Spike BA.1	Sino Biological Inc.	Cat# 40589-V08H26
Trimeric SARS-CoV-2 Spike BA.4/5	Sino Biological Inc.	Cat# 40589-V08H32
Trimeric SARS-CoV-2 Spike BA.2.75	Sino Biological Inc.	Cat# 40589-V08H36
Trimeric SARS-CoV-2 Spike BQ.1	Sino Biological Inc.	Cat# 40589-V08H41
Trimeric SARS-CoV-2 Spike XBB.1.16	Sino Biological Inc.	Cat# 40589-V08H48
RBD of the SARS-CoV-2 Spike Wuhan	Murae et al.[93]	N/A
RBD of the SARS-CoV-2 Spike BA.1	Murae et al.[93]	N/A
RBD of the SARS-CoV-2 Spike XBB.1.16	This study	N/A
hACE2-Fc	Murae et al.[93]	N/A
His-S1 spike protein	Ray Biotech	Cat# 230-01102
His-S2 spike protein	Ray Biotech	Cat# 230-01103

(*Continued on next page*)

Continued

REAGENT or RESOURCE	SOURCE	IDENTIFIER
D1146 peptide	Eurofins Genomics K.K.	GIVNNTVYDPLQPELDSF
E1146 peptide	Eurofins Genomics K.K.	GIVNNTVYDPLQPELESF
PBS	FUJIFILM Wako Pure Chemical Corp.	Cat# 166-23555
PEIpro® transfection reagent	Polyplus Transfection	Cat# 101000017
Kanamycin	FUJIFILM Wako Pure Chemical Corp.	Cat# 117-00961
G418	FUJIFILM Wako Pure Chemical Corp.	Cat# 074-06801
Bovine Serum Albumin fatty acid free	FUJIFILM Wako Pure Chemical Corp.	Cat# 011-15144
4%-Paraformaldehyde Phosphate Buffer Solution	NACALAI TESQUE, INC.	Cat# 09154-14
10% Tween 20	Bio-Rad Laboratories Inc.	Cat# 1610781
Sulfuric acid	FUJIFILM Wako Pure Chemical Corp.	Cat# 195-04706
1-Step™ TMB ELISA Substrate Solutions	Thermo Fisher Scientific	Cat# 34028
DMEM	FUJIFILM Wako Pure Chemical Corp.	Cat# 044-29765
Opti-MEM™	Thermo Fisher Scientific	Cat# 31985062
Vectashield Vibrance Antifade Mounting Medium with DAPI	Vector Laboratories Inc.	Cat# H-1700
PicaGene Meliora Star-LT Luminescence Reagent	TOYO B-NET Co., Ltd.	Cat# MLT100
EzWestLumi plus®	ATTO Corp.	Cat# WES-7120
ADCC Reporter Bioassay, Complete Kit	Promega corp.	Cat# G7015
Experimental models: Cell lines		
HEK 293T cells	ATCC	CRL-3216
HEK293/ACE2 cells	This study	N/A
VeroE6/TMPRSS2 cells	JCRB	JCRB1819
Raji cells	Promega corp.	Cat# G8701
ADCC Bioassay Effector Cells, V158 variant	Promega corp.	Cat# G7011
Recombinant DNA		
pcDNA3.1-spike/Wuhan	Yamamoto et al.[92]	N/A
pcDNA3.1-spike/D614G	Yamamoto et al.[92]	N/A
pcDNA3.1-spike/Alpha	Yamamoto et al.[92]	N/A
pcDNA3.1-spike/Delta	Yamamoto et al.[92]	N/A
pcDNA3.1-spike/BA.1	Yamamoto et al.[92]	N/A
pcDNA3.1-spike/BA.5.2	This study	GenBank: UPN16705.1
pcDNA3.1-spike/BA.2.75	This study	GenBank: USV68346.1
pcDNA3.1-spike/BA.5.2-K444T	This study	N/A
pcDNA3.1-spike/BA.2.75-V445P	This study	N/A
pcDNA3.1-spike/RaTG-13	This study	GenBank: MN996532
pcDNA3.1-spike/Khosta-2	This study	GenBank: MZ190138
pcDNA3.1-C-DYK-ACE2	GenScript Japan Inc.	Cat# MC_0101086
pcDNA3.1-C-DYK-TMPRSS2	This study	OHu13675D, GenScript Japan Inc.
pEGFP-C1	BD Biotech Clontech	N/A
pQCXIP-GFP1-10	Kodaka et al.[53]	Addgene 68715
pQCXIP-BSR-GFP11	Kodaka et al.[53]	Addgene 68716
pTG-Luc126	Rafique et al.[94]	N/A
phCMV-Gag-Pol 5349	Rafique et al.[94]	N/A

(*Continued on next page*)

Continued

REAGENT or RESOURCE	SOURCE	IDENTIFIER
Software and algorithms		
GraphPad Prism 9	GraphPad Software, Inc.	N/A
UCSF Chimera	Pettersen et al.[95]	N/A
ImageJ	National Institutes of Health	http://imagej.nih.gov/ij/
Jalview	Waterhouse et al.[96]	N/A
Adobe® Photoshop CS4 Extended software	Adobe Systems Inc.	N/A
Biacore X100 Evaluation Software	Cytiva	N/A
Other		
TC plate 12well	SARSTEDT	Cat# 83.3921
IsoPlate-96 TC white	ParkinElmer	Cat# 6005078
Costar® 96 well EIA/RIA Plate	Corning	Cat# 3590
4 well slide chamber	Corning	Cat# 354114
Sensor Chip CM5	Cytiva	#BR100399
amine coupling kit	Cytiva	#BR100050
Envision 2105	PerkinElmer	N/A
SpectraMax iD3	MOLECULAR DEVICE	N/A
BZ-X800	KEYENCE	N/A
ImageQuant LAS4000 mini-image analyzer	GE Healthcare Japan Corp.	N/A
Biacore X100	Cytiva	N/A

RESOURCE AVAILABILITY

Lead contact

Further information or requests should be directed to and will be fulfilled by the lead contact, Kohji Noguchi (noguchi-kj@rs.tus.ac.jp).

Materials availability

All materials, except for authentic viruses, in this study can be available upon reasonable request, or through commercially available sources.

Data and code availability

- All data reported in this paper can be made available upon reasonable request from the lead contact.
- This paper does not report any original code.
- Any additional information required to reanalyze the data reported in this paper is available from the lead contact upon request.

EXPERIMENTAL MODEL AND STUDY PARTICIPANT DETAILS

Animals for hybridoma production

Two 6-week-old female BALB/c mice were purchased from CLEA Japan (Tokyo, Japan) and housed under specific-pathogen-free conditions. All animal experiments were approved by the Animal Care and Use Committee of Tohoku University (permit number: 2019NiA-001). Each BALB/c mouse was intraperitoneally (i.p.) immunized with 100 μg of N-terminal His-tagged S1 spike protein of SARS-CoV-2 (Cat# 230–01102, Ray Biotech, Peachtree Corners, GA, USA) for the development of CvMab-6 or 100 μg of His-tagged S2 spike protein of SARS-CoV-2 (Cat# 230–01103, Ray Biotech) for the development of CvMab-62. Inject Alum (Thermo Fisher Scientific) was used for the first immunization. The procedure included three additional immunization procedures (100 μg/mouse), followed by a final booster i.p. injection (100 μg/mouse) 2 days before harvesting the spleen cells, which were subsequently fused with P3U1 cells using polyethylene glycol 1500 (PEG1500; Roche Diagnostics; Indianapolis, IN, USA). Hybridomas were grown in RPMI medium supplemented with hypoxanthine, aminopterin, and thymidine for selection (Thermo Fisher Scientific). The culture supernatants were screened using ELISA to detect SARS-CoV-2 S1 for the development of CvMab-6 or SARS-CoV-2 S2 for the development of CvMab-62. Clone CvMab-6 or clone CvMab-62 culture supernatants in hybridoma-SFM medium (Thermo Fisher Scientific) were purified using an Ab-Capcher (ProteNova, Kagawa, Japan).

Cell culture

HEK293T cells (ATCC, CRL-3216) and VeroE6/TMPRSS2 (JCRB, JCRB1819) cells were cultured at 37°C in Dulbecco's modified Eagle medium (DMEM) supplemented with 7.5% fetal bovine serum (FBS) and kanamycin (50 μg/mL). P3U1 (ATCC, CRL-1597) was cultured in a Roswell Park Memorial Institute (RPMI)-1640 medium (Nacalai Tesque, Kyoto, Japan), with 10% heat-inactivated FBS (Thermo Fisher Scientific, Waltham, MA, USA), 100 units/mL of penicillin, 100 μg/mL of streptomycin, and 0.25 μg/mL of amphotericin B (Nacalai Tesque). HEK293/ACE2 cells were generated by transfection of a human ACE2-DYK-expressing plasmid (Cat# MC_0101086, GenScript Japan, Tokyo, Japan) into HEK293 cells (ATCC, CRL-1573), and stable ACE2-expressing clones were isolated after G418 selection.

SARS-CoV-2 viruses

SARS-CoV-2 viruses, Wuhan strain (2019-hCoV/Japan/TY/WK-521/2020, GISAID ID: EPI_ISL_408667), Alpha variant B.1.1.7 (hCoV-19/Japan/QHN001/2020, GISAID ID: EPI_ISL_804007), Delta variant B.1.617.2 (hCoV-19/Japan/TY11-927/2021, GISAID ID: EPI_ISL_2158617), Omicron variant BA.1 (hCoV-19/Japan/TY38-873/2021, GISAID ID: EPI_ISL_7418017), Omicron variant BA.5.2.1 (hCoV-19/Japan/TY41-704/2022, GISAID ID: EPI_ISL_13241868), and Omicron variant BQ.1.1 (hCoV-19/Japan/TY41-796/2022, GISAID ID: EPI_ISL_15579783) were obtained from National Institute of Infectious Disease (Japan) and handled in biosafety level 3 (BSL-3) facilities.

METHOD DETAILS

Spike plasmid construction

The plasmid pUC57-2019-nCoV-S (human), containing synthetic cDNA to express SARS-CoV-2 spike protein with human codon optimization, was purchased from GenScript and cloned into the expression plasmid pcDNA3.1. Mutant spike cDNAs was synthesized using GenScript.[92]

Development of bispecific antibody

To generate each bispecific antibody, we first constructed an scFv of CvMab-6 (Cv6-scFv) or CvMab-62 (Cv62-scFv) by connecting the VH and VL cDNA of CvMab-6 or CvMab-62 with a linker sequence (GGGGSGGGGSGGGGS). Each scFv cDNA was further fused at the 3′ end of the heavy or light chain cDNA of CvMab-6 or CvMab-62, to create Bis1 (Cv62-scFv fused to the heavy chain of CvMab-6), Bis2 (Cv62-scFv fused to the light chain of CvMab-6), Bis3 (Cv6-scFv to the heavy chain of CvMab-62), or Bis4 (Cv6-scFv to the light chain of CvMab-62). In order to generate bispecific antibodies with bebtelovimab, we first constructed a single chain Fv (scFv) of bebtelovimab by connecting the V_L and V_H cDNA of bebtelovimab with a linker sequence (GGGGSGGGGSGGGGS). To generate humanized Bis-beb, the V_H cDNAs of humanized CvMab-62 and the C_H cDNA of human IgG_1 were cloned into the pCAG-Neo vector (FUJIFILM Wako Pure Chemical Corporation, Osaka, Japan). scFv cDNA of bebtelovimab was further fused at the 3′ end of the heavy chain cDNA of mouse or humanized CvMab-62. The V_L cDNA of humanized CvMab-62 and the C_L cDNA of the human kappa light chain were also cloned into the pCAG-Ble vector (FUJIFILM Wako Pure Chemical Corporation). The cDNA of each heavy and light chain was transduced into ExpiCHO-S cells using the ExpiCHO Expression System (Thermo Fisher Scientific). Each antibody was purified using an Ab-Capcher. For bispecific antibodies, the amino acid sequence can be conditionally disclosed upon request.

ELISA for antibody development

His-tagged S1 spike protein of SARS-CoV-2 (100 μg) or 100 μg of His-tagged S2 spike protein of SARS-CoV-2 was immobilized on Nunc Maxisorp 96-well immunoplates (Cat# 439454, Thermo Fisher Scientific) at 1 μg/mL for 30 min at 37°C. After washing with phosphate buffered saline (PBS) containing 0.05% Tween 20 (PBS-T; Nacalai Tesque), wells were blocked with 1% bovine serum albumin (BSA) in PBS-T for 30 min at 37°C. The plates were incubated with primary antibodies followed by peroxidase-conjugated anti-mouse immunoglobulin (1:1000; Agilent Technologies, Santa Clara, CA, USA). Finally, enzymatic reactions were performed using an ELISA POD substrate TMB kit (Cat# 05298-80, Nacalai Tesque). The absorbance at 655 nm was measured using an iMark microplate reader (Bio-Rad Laboratories, Berkeley, CA).

CvMab-6 epitope mapping

The 22 peptides from the S1-RBD sequence were synthesized using PEPScreen (Sigma-Aldrich, St. Louis, MO, USA). The cysteine in each peptide was converted into serine. The peptide sequences are listed in Table S1. The binding assay was performed using ELISA, as described above. Briefly, each peptide was immobilized on Nunc Maxisorp 96-well immunoplates at 1 μg/mL for 30 min at 37°C. After washing with PBS-T, wells were blocked with 1% BSA in PBS-T for 30 min at 37°C. The plates were then incubated with CvMab-6, followed by incubation with peroxidase-conjugated anti-mouse immunoglobulins (1:1000). Finally, enzymatic reactions were performed using an ELISA POD substrate TMB kit (Nacalai Tesque, Inc.). The absorbance was measured at 655 nm using an iMark microplate reader.

CvMab-62 epitope mapping

S2 deletion mutant cDNAs encoding the SARS-CoV-2 spike protein S2 region, as shown in Figure 2, were cloned into the pUC57 plasmid (GenScript Japan). Recombinant proteins were expressed by IPTG induction in *E.coli* JM109, and cell lysates were prepared. Anti-S2 antibody

reactivity to these S2 proteins was examined by western blot analysis using CvMab-62 and 1A9 (Cat# GTX632604, GeneTex, CA, USA) and a polyclonal anti-S2 antibody (Cat# 40590-T62, Sino Biological, Beijing, China).

Pseudotyped virus neutralization assay

Retrovirus-based pseudotyped virus production was performed as previously described.[93] Briefly, phCMV-Gag-Pol 5349 and reporter pTG-Luc126 plasmids[94] were co-transfected into HEK293T cells along with SARS-CoV-2 spike expressing plasmids using the PEIpro transfection reagent (Cat# 101000017, Polyplus Transfection, New York, NY). Medium was added the day after transfection. The cell supernatant containing pseudotyped virus was collected 72 h post-transfection, filtered through a 0.45 μm filter, and aliquoted to be stored at −80°C.

VeroE6/TMPRSS2 cells were seeded in 96-well white plates. The next day, antibodies were serially diluted in medium and mixed with pseudotyped viruses for 1 h at 37°C, and then added to the wells. For peptide competition assay, antibodies was preincubated with epitope peptide at 37°C for 30 min. After 3 days, the medium was removed. Cells were washed once with PBS and subsequently lysed using a luciferase assay reagent (Cat# MLT100, PicaGene Meliora Star-LT Luminescence Reagent; TOYO B-NET, Tokyo, Japan). Transduction was performed in triplicate in each experiment. The average and standard deviation (SD) were calculated, and reproducibility was confirmed by at least two independent biological experiments.

Authentic SARS-CoV-2 neutralization assay

VeroE6/TMPRSS2 cells were cultured in DMEM (Cat# 044–29765, Fujifilm Wako Pure Chemical Industries, Osaka, Japan) supplemented with 10% (v/v) heat-inactivated FBS (Cat# FBS-12A, Capricorn Scientific GmbH, Ebsdorfergrund, Germany), 100 U/ml penicillin G, 100 μg/mL streptomycin sulfate (Cat# 26253-84, Nacalai Tesque), and 1 mg/mL G418 (Cat# 09380-86, Nacalai Tesque). One day before SARS-CoV-2 infection, the cells were seeded in a 48-well plate (Cat# 3548, Corning, Glendale, AZ, USA) at a density of 5×10^4 cells/well. Viruses (WT, 0.001 TCID50/cell; Alpha, 0.01 TCID50/cell; Delta, 0.1 TCID50/cell; Omicron BA1, 0.1 TCID50/cell; and Omicron BA5.2.1, 0.001 TCID50/cell) were preincubated with CvMab-62, Bis1, Bis2, Bis3, Bis4, bebtelovimab, Bis-Beb, mouse IgG (Cat# 140–09511, Fujifilm Wako Pure Chemical Industries; Cat# 1015-000-003, Jackson ImmunoResearch, West Grove, PA, USA), humanized Bis-beb, or human IgG (Jackson, Cat# 009-000-003) at 37°C for 30 min. The mixtures were added to the cell monolayers and the cells incubated for 2 h. After removing the antibody-virus mixtures, the cells were washed with PBS and cultured in normal growth medium in the presence of antibodies for 24 h. Viral RNA copies in the culture supernatant and cells were determined as described below.

Quantification of viral RNA

Total RNA from the culture supernatant and cells was extracted using the Viral RNA/Viral Nucleic Acid Mini Kit (Cat# FAVNK 001–2, Favorgen Biotech, Pingtung City, Taiwan) and the Tissue Total RNA Purification Mini Kit (Cat# FATPK 001–2, Favorgen Biotech), respectively, according to the manufacturer's instructions. Viral RNA copies were quantified via real-time RT-PCR analysis using the THUNDERBIRD Probe One-step qRT-PCR Kit (Cat# QRZ-101, Toyobo, Osaka, Japan). SARS-CoV-2-specific primers (NIID_2019-nCOV_N_F2; 5′-AAATTTTGGGGACCAG GAAC-3′, NIID_2019-nCOV_N_R2; 5′-TGGCAGCTGTGTAGGTCAAC-3′) and probe (NIID_2019-nCOV_N_P2; 5′-FAM-ATGTCGCGCAT TGGCATGGA-BHQ-3′) were purchased from Eurofins Genomics (Tokyo, Japan).

Immunoblotting

The cells were lysed using radioimmunoprecipitation assay (RIPA) buffer (Cat# 16488-34, Nacalai Tesque) containing protease inhibitors. Proteins were separated using SDS-PAGE and transferred to Immobilon-P membranes (Cat# IPVH00010, EMD Millipore, Billerica, MA, USA). After blocking with 5% milk in PBS-T for 1 h, membranes were incubated with primary antibodies at 4°C overnight. Membranes were then washed with PBS-T and incubated with secondary antibodies for 2 h. Membranes were washed again with PBS-T and immunoblot signals were developed using EzWestLumi plus (Cat# WES-7120, ATTO, Tokyo, Japan) and recorded using an ImageQuant LAS4000 mini-image analyzer (GE Healthcare Japan, Tokyo, Japan). The antibodies used were as follows: anti-spike antibody 1A9 (Cat# GTX632604, GeneTex, CA, USA), anti-cleaved spike (Ser 686) antibody (Cat# 84534, Cell Signaling Technology, Massachusetts, USA), anti-GAPDH 3H12 (Cat# 171-3, Medical & Biological Laboratories, Aichi, Japan), goat anti-mouse IgG antibody conjugated with horseradish peroxidase (Cat# SA00001-1, Proteintech Group, Rosemont, USA), donkey anti-rabbit IgG antibody conjugated with horseradish peroxidase (Cat# NA934, Cytiva, Tokyo, Japan).

Immunofluorescence microscopic analysis

HEK 293T cells were seeded in a poly D-lysine-coated four well slide chamber (Cat# 354114, Corning, Corning, NY, USA) and transfected with the SARS-CoV-2 spike protein the following day. Forty-eight hours after transfection, the cells were fixed in 4% paraformaldehyde (Cat# 09154-14, Nacalai tesque, Inc.) for 10 min and blocked with 1% BSA/PBS for 30 min. The cells were then incubated with primary antibodies (CvMab-6 and CvMab-62) at a concentration of 10 μg/mL in 1% BSA/PBS for 2 h at room temperature and washed three times with PBS. Next, the cells were incubated with goat anti-mouse IgG (H + L) cross-adsorbed Alexa Fluor 488 (Cat# A-11001, Thermo Fisher Scientific, Carlsbad, CA) diluted × 2000 in 1% BSA/PBS at room temperature for 1 h and washed again with PBS three times. Vectashield Vibrance Antifade Mounting Medium (Cat# H-1700, Vector Laboratories, CA, USA) was added, and the cells were incubated at room temperature for 1 h. Images

were captured using a BZ-9000 microscope (Keyence, Osaka, Japan). Two-dimensional TIFF images were merged using Adobe Photoshop CS4 Extended software (Adobe Systems Inc., San Jose, CA, USA).

Cell-cell fusion assay

To prepare the effector cells, HEK 293T cells were co-transfected with EGFP and SARS-CoV-2 spike protein-expressing plasmids. Cells were collected 48 h after transfection and treated with antibodies at a final concentration of 100 μg/mL at 37°C for 30 min, then added to VeroE6/TMPRSS2 cells as target cells and co-cultured at 37°C for 3 h. After incubation, five fields were randomly selected in each well, and images were captured using a fluorescence microscope BZ-X800 (Keyence). Images were analyzed using ImageJ software to quantify the GFP area. To assess TMPRSS2 dependence of cell-cell fusion inhibition, we used HEK293T cells co-transfected with split GFP1-10 and SARS-CoV-2 spike-expressing plasmids as effector cells and HEK293T cells co-transfected with split GFP11 and TMPRSS2 expressing plasmids as target cells, 48 h after transfection.[52] The remaining steps were performed as described previously. After the cell-cell fusion assay, cell lysates were collected and used for western blotting to confirm the TMPRSS2-dependent cleavage of the spike protein.

ELISA for binding affinity calculation

Wells of 96-well microtiter plates were coated with 1 μg/mL purified recombinant SARS-CoV-2 Trimeric Spike ECD and RBD (Spike WT; Cat# 40589-V08H4, Spike BA.1; Cat# 40589-V08H26, Spike BA.4/5; Cat# 40589-V08H32, Spike BQ.1; Cat# 40589-V08H41, Spike BA.2.75; Cat#40589-V08H36, RBD BQ.1; Cat# 40589-V08H143, Sino Biological, Beijing, China) at 4°C overnight. Plates were blocked with 1% BSA in PBS-T for 1 h. Antibodies were diluted in blocking buffer, added to the wells, and incubated for 2 h at room temperature. For peptide competition assay, CvMa-62 was preincubated with epitope peptide at 37°C for 30 min. The bound antibodies were detected using goat anti-mouse IgG antibody conjugated with horseradish peroxidase (Proteintech Group) and TMB substrate (Cat# 34028, 1-Step TMB ELISA Substrate Solutions, Thermo Fisher Scientific, Carlsbad, CA). Color development was monitored, 2 M sulfuric acid was added to stop the reaction, and the absorbance was measured at 450 nm using a multi-mode plate reader SpectraMax iD3 (Molecular Devices, CA, USA).

ELISA for *in vitro* RBD and ACE2 neutralization assay

Wells of 96-well microtiter plates were coated with 1 μg/mL recombinant hACE2-Fc at 4°C overnight. Plates were blocked with 1% BSA in PBS containing 0.05% PBS-T for 2 h. Antibodies and recombinant His-tagged SARS-CoV-2 Spike trimeric ectodomain or RBD proteins were mixed and incubated for 1 h at room temperature. The antibodies and RBD mixture were added to the wells and incubated for 2 h at room temperature. Trimeric spike ectodomain or RBD bound to ACE2 were detected using Anti-His-tag mAb-HRP-DirecT (Cat# D291-7, Medical & Biological Laboratories, Tokyo, Japan) and TMB substrate (1-Step TMB ELISA Substrate Solutions, Thermo Fisher Scientific, Carlsbad, CA). Color development was monitored, 2 M sulfuric acid was added to stop the reaction, and the absorbance was measured at 450 nm using a multi-mode plate reader SpectraMax iD3 (Molecular Devices).

The surface plasmon resonance (SPR) experiments

To measure the affinity of each antibody for the antigen (trimeric BQ.1.1 and BA. 4/5 spike ectodomains), we performed SPR analysis using Biacore X100 (Cytiva, Marlborough, MA, USA). HBS-EP + buffer (10 mM HEPES [pH 7.4], 150 mM NaCl, 3 mM EDTA, and 0.05% v/v surfactant P20) and MBS-EP + buffer (10 mM MES [pH 5.5], 150 mM NaCl, 3 mM EDTA, and 0.05% v/v surfactant P20) were used as running buffers. One hundred glycine HCl (pH 1.5) and 50 mM NaOH were used as the dissociation buffer. Anti-His tag mAb (Cat# D291-3, Medical & Biological Laboratories) was immobilized on a Sensor Chip CM5 (Cat# BR100399, Cytiva) using an amine coupling kit (Cat# BR100050, Cytiva) according to the manufacturer's standard amine coupling protocol. The level of immobilized trimeric spike ectodomain in active flow cells reached approximately 500 response units. Antibodies were serially diluted (0.11, 0.33, 1.0, 3.0, and 9.0 μg/mL) in the running buffer. The single-binding cycles were injected sequentially with increasing concentrations over both the ligand and reference surfaces. The reference surface, which was an unmodified flow cell, was used to correct systematic noise and instrumental drift. To determine ka, kd, and KD values, the sensorgrams were globally fitted using a 1:1 binding model and analyzed using Biacore X100 Evaluation Software.

Structural modeling of the spike protein

Structural modeling was performed using the 3D mol.js software (https://3 dmol.csb.pitt.edu/), UCSF Chimera,[95] and Jalview.[96] Modeling of 'SARS-CoV-2 Spike RBD bound with ACE2 (6M0J)' was performed in 3D mol.js software and used in Figure 2D. Meanwhile, modeling of 'LY-CoV1404 against SARS-CoV-2 RBD (7MMO)' and 'SARS-CoV-2 Spike protein prefusion form (6XR8) and postfusion form (6XRA)' were performed in UCSF Chimera and used in Figures 6E, 9E, and S6.

Antibody-dependent cellular cytotoxicity (ADCC) assay

ADCC was quantified using the ADCC Reporter Bioassay Complete Kit (Promega, Cat# G7015, Madison, WI, USA) as previously described.[97,98] Briefly, 5×10^4 ADCC Bioassay Target Cells (Raji, Cat# G8701) were co-cultured with 5×10^4 ADCC Bioassay Effector Cells (Jurkat cells stably expressing the FcγRIIIa receptor, V158 variant, Cat# G7011) in the presence or absence of control antibody (Anti-CD20, Cat# GA1130) at the indicated concentration. The luminescence signals were measured after 18 h of incubation using an EnVision multilabel plate reader (PerkinElmer, 2104-0020, MA, USA). Using this system, HEK293T cells that transiently expressed the SARS-CoV-2 spike were co-cultured with

ADCC Bioassay Effector Cells in the presence or absence of each anti-spike antibodies. After 18 h of culture, luminescence signals were measured. ADCC was measured as the fold induction of luciferase activity compared to the ''no antibody'' condition.

QUANTITATIVE AND STATISTICAL ANALYSIS

Inhibition concentrations (IC_{50} values) during the neutralization assays and KD values in the ELISA binding assays were determined. Data visualization and statistical analyses were performed using GraphPad Prism 9 (GraphPad Software, Inc., Boston, MA, U.S.A). Statistical differences were determined using an unpaired t-test, or a one-way ANOVA followed by the Bonferroni test post hoc test (group ≥ 3). Data are presented as the means $\pm$ SD from triplicated samples, minimum, and reproducibility was confirmed by a minimum of two independent biological experiments. Statistical significance was defined as a p value <0.05, $*p < 0.05$, $**p < 0.01$, and $***p < 0.001$. Multiple sequence alignments of spike proteins were performed using Clustal Omega software (https://www.ebi.ac.uk/Tools/msa/clustalo/). Quantification of the GFP signal images was performed using ImageJ software (NIH). Where applicable, the statistical parameters are reported in the figure legends.